

Thermal Contact Conductance in Bolted Joints

by

ALBIN K J. HASSELSTRÖM
U. ESKIL NILSSON

Diploma work No. 85/2012
at Department of Materials and Manufacturing Technology
CHALMERS UNIVERSITY OF TECHNOLOGY
Gothenburg, Sweden

Diploma work in the Master programme Product Development & Applied Mechanics

Performed at: RUAG Space AB
Solhusgatan 11, 412 76 Gothenburg

Supervisor(s): Karin Woxlin
RUAG Space AB
Solhusgatan 11, 412 76 Gothenburg

Examiner: Johan Ahlström
Department of Materials and Manufacturing Technology
Chalmers University of Technology, SE - 412 96 Gothenburg

Thermal Contact Conductance in Bolted Joints

ALBIN K J. HASSELSTRÖM

U. ESKIL NILSSON

© ALBIN K J. HASSELSTRÖM, U. ESKIL NILSSON, 2012.

Diploma work no 85/2012

Department of Materials and Manufacturing Technology

Chalmers University of Technology

SE-412 96 Gothenburg

Sweden

Telephone + 46 (0)31-772 1000

Abstract

Determining thermal contact conductance in bolted joints is a major challenge when designing for space application. The lack of heat transfer through convection enforces the need for full understanding of thermal contact conductance, and the influencing physical parameters. Due to the uncertain variance of pressure distribution in a bolted joint, determination of thermal contact conductance becomes difficult. At the time of this thesis, models describing thermal contact conductance in bolted joints, were limited.

In accordance with RUAG Space, vacuum experiments on generic rods as well as bolted joints were executed. Measured interface temperature drops were used as reference in iterative finite volume analyses, developed to estimate the thermal contact conductance.

Results were achieved for the relationship between interface pressure and thermal contact conductance in nickel-plated aluminum joints. Available theoretical models were found to vary strongly in estimation of thermal contact conductance. Performing experiments adapted to the specific application was therefore found to be essential for gaining knowledge about the actual thermal contact conductance. Experiments on bolted joints gave information about the total thermal contact conductance and its dependence on several important design parameters, including bolt torque, number of bolt, surface roughness and joint material. The overall results coincided with theory.

In conclusion, the thesis puts forth a new method of thermal contact conductance estimations in bolted joints by a combination of empirical test data and finite volume analyses. This method was concluded to result in more accurate estimation of thermal contact conductance in bolted joints, compared to older studies.

Keywords: *thermal contact conductance, bolted joint, thermal interface material, vacuum environment*

Acknowledgements

"You are working on a very complex problem from both a mechanical and a thermal perspective. There are no simple solutions or models."

Michael M. Yovanovich

We would like to thank our supervisor Karin Woxlin for her guidance and support. Many thanks to the staff of RUAG Space for help with using the vacuum chamber, electronic equipment and practical issues of all kinds. We would also like to thank our examiner Johan Ahlström for his useful input, adding important quality to the thesis.

Albin Hasselström & Eskil Nilsson, Gothenburg 8/6-12

Contents

1	Introduction	1
1.1	Objective	2
1.2	Limitations	2
2	Review of Literature	3
2.1	Theory of Thermal Contact Conductance	3
2.2	Factors Influencing Thermal Contact Conductance	5
2.3	Models for Thermal Contact Conductance	5
2.3.1	Useful Formulas and Correlations	6
2.3.2	Elastic Models	8
2.3.3	Plastic Models	9
2.3.4	Relationship for Relative Contact Pressure	11
2.4	Bolted Joints	12
2.4.1	Relationship between Tightening Torque and Bolt Axial Force	13
2.4.2	Relationship for Pressure Distribution in Bolted Joints	13
2.5	Enhancement of Thermal Contact Conductance	16
2.5.1	Thermal Interface Material	16
2.5.2	Geometric and Application Optimization	18
2.6	Testing of Thermal Contact Conductance	20
2.6.1	Cylinder Experiment	20
2.6.2	Bolted Joint Experiment	21
3	Method	25
3.1	Layout of Experiments	25
3.1.1	Varied Parameters in Bolted Joint Experiment	26
3.1.2	Varied Parameters in Cylinder Joint Experiment	27
3.2	Setup of Experiments	27
3.2.1	Bolted Joint Experiment	27
3.2.2	Cylinder Joint Experiment	29
3.2.3	Placement of Thermocouples	31

3.2.4	Equipment	31
3.3	Procedure of Experiments	31
3.4	Estimation of Heat Losses	32
3.4.1	Radiation Losses From Heater and Top Specimen	32
3.4.2	Conduction and Radiation Losses in Cables	33
3.4.3	Conduction Losses Through Insulation in Cylinder Experiment	34
3.5	Measurement of Physical and Material Parameters	35
3.5.1	Pressure Distribution	35
3.5.2	Surface Roughness	35
3.5.3	Microhardness	36
3.6	Estimation of Thermal Contact Conductance	36
3.6.1	Bolted Joint Experiment	36
3.6.2	Cylinder Joint Experiment	38
3.7	Error analysis	39
3.7.1	Uncertainty in Thermal Conductivity of Materials	39
3.7.2	Uncertainty in Heat Input in Bolted Joint Experiment	40
3.7.3	Error in Thermocouples	40
3.7.4	Uncertainty in Thermocouple Position	40
3.8	Testing of Thermal Interface Material	40
4	Result	43
4.1	Pressure Distribution in Bolted Joints	43
4.2	Thermal Contact Conductance	46
4.2.1	Bolted Joint Experiment	46
4.2.2	Cylinder Joint Experiment	49
4.3	Evaluation of Analytical Models	49
4.4	Evaluation of Thermal Interface Material	50
5	Conclusion	53
5.1	Pressure Distribution in Bolted Joints	53
5.2	Bolted Joint Experiment	53
5.2.1	Number of Bolts	53
5.2.2	Surface Roughness	54
5.2.3	Applied Torque on Bolts	54
5.2.4	Joint Component Materials	55
5.2.5	Thermal Interface Material	55
5.3	Analytical Model Evaluation	55
	Bibliography	60
A	Selection of Thermal Interface Material	61

B	Experiment Results	63
B.1	Bolted Joint Experiments	63
B.2	Cylinder Joint Experiments	66
C	Estimation of Total Thermal Conductance in Bolted Joint Experiments	69
C.1	Cylinder Joint Experiment	70
D	Microhardness Measurements	77
E	Roughness Measurements	79
F	Model Parameters	81

Nomenclature

A	Area	[m ²]
C	Thermal contact conductance	[W/K]
E	Modulus of elasticity	[Pa]
F	Force	[N]
FD	Flatness deviation	[m]
H_c	Surface microhardness	[Pa]
H_V	Vickers microhardness	[Pa]
h_c	Thermal contact conductance per unit area	[W/m ² K]
h_j	Total joint conductance per unit area	[W/m ² K]
h_g	Gap conductance per unit area	[W/m ² K]
h_r	Radiative conductance per unit area	[W/m ² K]
k	Thermal conductivity	[W/mK]
k_s	Effective thermal conductivity	[W/mK]
M	Torque	[Nm]
m	Absolute surface slope	[-]
m_s	Effective mean absolute surface slope	[-]
m'	RMS surface slope	[-]
m'_s	Effective RMS surface slope	[-]
P	Pressure	[Pa]
Q	Heat flow rate	[W]
q	Heat flow rate per unit area	[W/m ²]
R_a	Arithmetic average of absolute values of surface roughness	[m]
R_j	Thermal contact resistance	[K/W]
r	Contact radius	[m]
S_Y	Yield Strength	[Pa]
T	Temperature	[K]
T_m	Mean joint temperature	[K]
ΔT	Joint temperature drop	[K]
α	Coefficient of Linear Thermal Expansion	[1/K]
δ	Gap thickness	[m]
ϵ	Emissivity	[-]
μ	Coefficient of friction	[-]
σ	RMS surface roughness	[m]
σ_s	Effective RMS surface roughness	[m]
τ	Bolt torque	[Nm]
ν	Poisson's ratio	[-]

1

Introduction

In satellites, heat generated from electronic components must be transferred to the outer surface of the structure and then radiated to the surrounding in order to keep the temperature of the electronic components within acceptable levels. Since satellites are operating in a vacuum environment, no heat can be transferred by convection, which is a customary component of ordinary cooling systems. Therefore, thermal management is considered a key issue in spacecraft design.

Generated heat in a satellite is mainly transferred by conduction from the electronic components out to the surface structure of the satellite. This thermal system consists of a series of components joined together, most commonly with bolted joints. The conductivity of each material is usually very well known. However, the ability for two mating materials to transfer heat over their contacting surfaces is complicated to determine. This ability is called thermal contact conductance.

Several geometrical, physical and material parameters influence the thermal contact conductance. Since the 1960's, great effort has been put into theoretical and empirical determination of correlations for thermal contact conductance in a vacuum environment. However, most of these models have been developed for two solid surfaces pushed together with a constant, well-known pressure.

The issue becomes more complex as plates are joined together with bolts. Some empirical tests have been performed, determining various parameters' influence on thermal contact conductance. The applicability of results are however limited to geometrical designs and conditions similar to those of the performed empirical tests.

This master's thesis is performed in collaboration with RUAG Space. One of RUAG Space's main product groups is electronic equipment for space applications. The electronic components are typically mounted on frames that are bolted into a chassis of aluminum. To be able to predict the thermal performance of the system, the thermal contact conductance in bolted joints needs to be known.

1.1 Objective

This master thesis aims at increasing the confidence in performing thermal analysis on specific RUAG Space products with respect to bolted joints. The work will consist of three parts:

1. Identification and evaluation of available theoretical and empirical models for thermal contact conductance between two solids. This includes all relations necessary from controllable inputs to resulting thermal contact conductance.
2. Design and execution of empirical tests, measuring the thermal contact conduction in chosen components. Selection of relevant input parameters to vary in the tests is included in the design process. The measurements will subsequently be used for evaluation of identified models, aiming at a recommendation of an improvement over the currently used model.
3. Investigation of ways of improving the thermal performance of bolted joints, aiming towards recommendations of design elements with increased system performance.

Based on the identified objectives of this master thesis, the following set of questions are to be answered:

- How do different parameters influence resulting thermal contact conductance of bolted joints?
- In what ways can the thermal performance of bolted joints be improved? What is the quantitative improvement in thermal contact conductance of recommended design changes?

1.2 Limitations

To confine the thesis the following limitations are chosen:

- The master thesis will only investigate bolted joint designs that are most relevant for RUAG Space. Hence, the types of bolted joint systems to be analyzed will be determined at an early state to narrow down and focus the analysis.
- Parameters with a low influence on thermal contact conductance of bolted joints will be dismissed from further analysis, thereby focusing the efforts on primary, empirically testable parameters.
- Certain parameters influencing the thermal contact conductance might not be feasible to change. In explanation, parameters considered to be superfluous by RUAG Space, will be dismissed from further analysis.
- The values of investigated parameters are limited to the actual range of values experienced by the products in real-world applications.
- Restrictions on testing equipment might enforce limitations in parameter choices.

2

Review of Literature

This chapter will present relevant literature that has been reviewed. The chapter starts with the basic theory of thermal contact conductance. This is followed by a description of the most important factors and established models for thermal contact conductance. The last section of the chapter investigates complications of thermal contact conductance in bolted joints, as opposed to thermal contact conductance between two flat plates with constant interface pressure.

2.1 Theory of Thermal Contact Conductance

Fourier's law of heat conduction in one dimension is given by

$$q_x = -k \frac{dT}{dx} \quad (2.1)$$

where q_x is the heat flow in the x -direction, k is the thermal conductivity of the material and dT/dx is the temperature gradient in the x -direction. It states that the heat flow per area unit in a given material is proportional to the temperature gradient. Heat flux over an interface between two surfaces in contact is subjected to a thermal contact resistance, defined as

$$R_j = \frac{\Delta T}{Q} = \frac{\Delta T}{qA} \quad (2.2)$$

As can be seen, the thermal contact resistance is defined as the ratio between the temperature drop over the interface, ΔT , and the total heat flux over the interface, Q . The thermal contact resistance causes a drop in temperature over the interface, illustrated in Figure 2.1. The main reason for the contact resistance is that the real contact area between the two contacting materials is just a small fraction of the apparent contact area, see Figure 2.2. The fraction between actual and apparent area, A_r/A_a , depends on several parameters such as surface roughness, surface hardness and contact pressure.

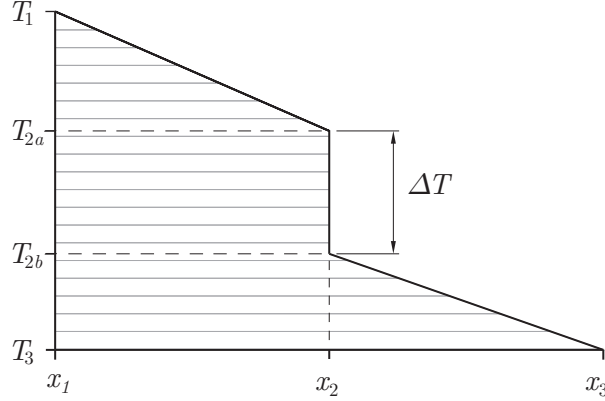


Figure 2.1: Temperature drop in joint interface located at $x = x_2$.

The joint thermal conductance is defined as the inverse of the resistance, given by

$$h_j = \frac{1}{R_j A} = \frac{q}{\Delta T} \quad (2.3)$$

There are three contributions to the joint conductance. Contact conductance, h_c , is the thermal conduction between contacting surfaces of the two interface materials. Gap conductance, h_g , is the conduction through the small, gas-filled gaps between the two materials. It is assumed to be gas conduction and not gas convection due to the small length scale of the gaps. Radiative conductance, h_r , is the thermal radiation between the two materials. All these three contributions to the joint conductance work in parallel, and the joint conductance can therefore be decomposed as

$$h_j = h_c + h_g + h_r \quad (2.4)$$

In space, which is a vacuum environment, there is no gas in the gaps between the two contacting materials and gap conductance can therefore be dismissed, $h_g = 0$. The radiative conductance depends strongly on the interface temperature. For interface temperatures below 600°C , radiation heat transfer over the interface can be assumed to be negligible [1], $h_r = 0$. For vacuum conditions and temperatures below 600°C , the contact conductance can therefore be assumed to equal the joint thermal conductance,

$$h_c = h_j = \frac{q}{\Delta T} \quad (2.5)$$

The total thermal contact conductance is given by

$$C_c = \frac{Q}{\Delta T} \quad (2.6)$$

2.2 Factors Influencing Thermal Contact Conductance

Several factors are considered to influence the thermal contact conductance of a joint in vacuum. Some of these factors involve properties of the two mating materials and some are external variable parameters. The parameters below have been addressed as influential [2][3].

Geometry of the contacting solids

Geometric parameters includes surface roughness (R_a or σ), flatness deviation (FD) and asperity slope (m or m').

Pressure (P)

The pressure between the contacting surfaces is generally deemed to have strong influence on the thermal contact conductance.

Gap thickness (δ)

This parameter describes the average gap distance between the contacting surfaces.

Thermal conductivity of the contacting materials (k)

The conductivity of the contacting materials, and the interface material if present, influences the thermal contact conductance.

Surface hardness (H_c) or yield strength (S_Y) of the contacting materials

This influences the plastic deformation of the surface peaks of the softer material.

Modulus of elasticity of the contacting solids (E)

This affects the elastic deformation of the contacting surfaces.

Average temperature of the interface (T_m)

This influences the physical properties of the contacting materials.

Linear coefficient of thermal expansion (α)

This parameter can, in conjunction with deviation from the average temperature of the interface, influence the behavior of the interface.

Thermal Interface Material

Interstitial material, such as foil, coating or grease, placed between the two surfaces of the joint with the purpose of increasing or decreasing the thermal conductance of the joint.

2.3 Models for Thermal Contact Conductance

The need for ways to quantify thermal contact conductance in practical applications has induced various analytical and empirical studies. Therefore, several mathematical models for calculating thermal contact conductance have been established. Different models use different input parameters, most of them described in the section above. This section will address some of these already established models and compare them.

First, commonly used relationships between material parameters and some correlations between material parameters will be presented. This will be followed by a review of existing thermal contact conductance models.

Generally, two types of models for thermal contact conductance exists. One set of models assumes elastic deformation while the other allows for plastic deformation when two solids are pressed together. Models of both types are presented below.

2.3.1 Useful Formulas and Correlations

The set of equations below define parameters and established correlations between the parameters that are often used in thermal contact conductance models. The effective thermal conductivity is given by [4]

$$k_s = \frac{2k_1k_2}{k_1 + k_2} \quad (2.7)$$

where the subscripts 1 and 2 correspond to the two materials of the joint.

Two commonly used expressions for describing the roughness of a surface are the arithmetic average of roughness, R_a , and the RMS¹ roughness, σ . These parameters are defined as

$$R_a = \frac{1}{L} \int_0^L |y(x)| dx \quad (2.8)$$

$$\sigma = \sqrt{\frac{1}{L} \int_0^L y^2(x) dx}$$

where $y(x)$ is the distance from the mean plane of the surface and L is the length of the trace. If assuming that the surface has a Gaussian distribution of asperities, then R_a and σ are related according to [5]

$$\sigma = \sqrt{\frac{\pi}{2}} R_a \approx 1.25 R_a \quad (2.9)$$

Another commonly used surface parameter is the absolute average asperity slope, m . Similarly, the absolute average asperity slope, m , and the RMS asperity slope, m' , are related according to [5]

$$m' = \sqrt{\frac{\pi}{2}} m \approx 1.25 m \quad (2.10)$$

assuming the surface has a Gaussian distribution of asperities. Since the two surfaces of a joint can have different roughnesses and asperity slopes, so called effective values are often used in mathematical models for thermal contact conductance. The effective RMS surface roughness is given by [4]

$$\sigma_s = (\sigma_1^2 + \sigma_2^2)^{1/2} \quad (2.11)$$

¹Root Mean Square

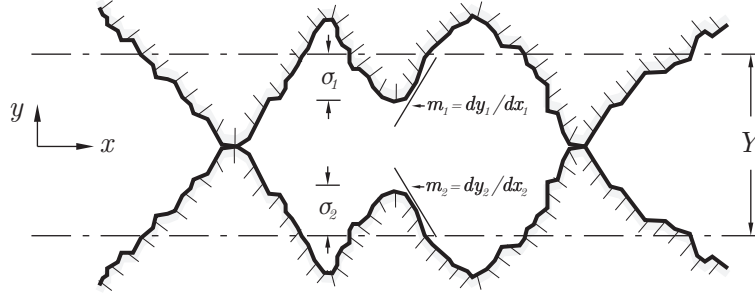


Figure 2.2: Illustration of two contacting surfaces, showing asperities and graphical representations of the absolute surface slope m and the RMS surface roughness σ .

The effective absolute mean asperity slope is given by [4]

$$m_s = (m_1^2 + m_2^2)^{1/2} \quad (2.12)$$

An illustration of two contacting surfaces are given in Figure 2.2, with graphical representations of σ and m .

A number of relations have been proposed between asperity slope and surface roughness, in order to limit the amount of surface parameters necessary to measure. Lambert and Fletcher proposed [6]

$$m = 0.076(\sigma \cdot 10^6)^{0.52} \quad (2.13)$$

suggesting a maximum uncertainty of plus/minus a factor of two. Antonetti, White and Simons [5] present a correlation established by Tanner and Fahoum [7], given by

$$m' = 0.208(R_a \cdot 10^6)^{0.4}, \text{ or} \quad (2.14)$$

$$m = 0.152(\sigma \cdot 10^6)^{0.4}$$

Antonetti, White and Simons propose another correlation [5], given by

$$m' = 0.183R_a^{0.743}, \quad R_a \leq 1.6\mu\text{m}, \text{ or} \quad (2.15)$$

$$m = 0.124\sigma^{0.743}, \quad \sigma \leq 2.0\mu\text{m}$$

Equation (2.9) and (2.10) are used to convert R_a and m' to σ and m . The three proposed correlations above, given by Equations (2.13), (2.14) and (2.15), were presented and compared in [8], where it was concluded that the uncertainties of the correlations were high.

2.3.2 Elastic Models

In this section, theoretical and empirical models for thermal contact conductance which assumes elastic deformation are presented. Assuming elastic deformation generally gives a model that depends on the modulus of elasticity of the contacting materials.

Fletcher and Gyrog, 1970

The following formulas below for calculating thermal contact conductance have been suggested by Fletcher and Gyrog in 1970 [3], and was also part of the European Space Agency's recommendations in 1989 [9]. This model relates material properties, surface finish, contact pressure and mean joint temperature to resulting contact conductance. The authors also compared the empirically determined model on empirical data from other studies and concluded an average overall error of less than 24%. The thermal contact conductance is given by

$$h_c = \frac{k_s}{\delta_0} \left[5.22 \cdot 10^{-6} \frac{\delta_0}{r} + 0.036 \frac{P}{E} \alpha T_m \right]^{0.56} \exp \left[170 \frac{P \alpha T_m r}{E \delta_0} \right] \quad (2.16)$$

where δ_0 is the gap thickness parameter, α is the coefficient of linear thermal expansion, T_m is the joint interface temperature, P is the pressure, E is the modulus of elasticity and r is the radius of the cylindrical joint interface. The gap thickness parameter is given by

$$\delta_0 = 5.194 \cdot 10^{-7} + 8.060 \cdot 10^{-2} s - 6.220 \cdot 10^{-2} s^2 + 2.108 \cdot 10^{-6} s^3 \quad (2.17)$$

where s is a surface parameter defined as

$$s = (FD + 2R_a)_{\text{rough}} - \frac{1}{2} (FD + 2R_a)_{\text{smooth}} \quad (2.18)$$

where FD is the flatness deviation and R_a is the surface roughness. The indices rough and smooth above denotes parameters for the rougher and the smoother surface if the joint consists of surfaces with different surface finishes. It should be noted that the European Space Agency [9] presents an incorrect version of Equation (2.17), since it does not correctly correspond to the original version in imperial units by Fletcher and Gyrog in [3].

Mikic, 1974

Mikic analytically derived several expressions for thermal contact conductance, considering the case of plastic or elastic deformation [10]. Assuming elastic deformation, the proposed thermal contact conductance model is given by

$$h_c = 1.55 \frac{k_s m_s}{\sigma_s} \left(\frac{P \sqrt{2}}{E' m_s} \right)^{0.94} \quad (2.19)$$

where E' is calculated from the modulus of elasticity E and the Poisson's ratio ν , given by

$$E' = \frac{E_1 E_2}{E_2(1 - \nu_1^2) + E_1(1 - \nu_2^2)} \quad (2.20)$$

Mikic concludes that h_c is weakly influenced by m_s ($h_c \sim m_s^{0.06}$), and that Equation (2.19) can be simplified using $m_s = 0.1$, the average for blasted surfaces, with a relatively small error. The elastic equation for h_c is then given by

$$h_c = 1.9 \frac{k_s}{\sigma_s} \left(\frac{P}{E'} \right)^{0.94} \quad (2.21)$$

Above formula has a high degree of practicality since only the RMS surface roughness and the pressure needs to be measured, provided material data such as conductivity etc. is available.

It should be noted that at least three other formulas have been developed that is similar to Equation (2.19) but with different numerical constants (1.55 and 0.94); Greenwood, and Williamson in 1966 [11], Onions and Archard in 1973 [12], Bush, Gibson and Thomas in 1975 [13]. All these models have been presented and compared against experimental data in [14].

2.3.3 Plastic Models

In this section, theoretical and empirical models for thermal contact conductance which assumes plastic deformation are presented. Assuming plastic deformation generally gives a model that depends on the surface hardness of the contacting materials.

Cooper, Mikic and Yovanovich, 1969

A model for thermal contact conductance has been suggested by Cooper, Mikic and Yovanovich [4]. Using a theoretical framework, a dimensionless relationship between applied pressure, material properties and thermal contact conductance was established, given by

$$\frac{h_c \sigma}{k_s m} \propto \frac{P}{H_c} \quad (2.22)$$

By fitting the above relationship to experimental data, the proposed model was

$$h_c = 1.45 \frac{k_s m_s}{\sigma_s} \left(\frac{P}{H_c} \right)^{0.985} \quad (2.23)$$

where the microhardness H_c is the lesser of the contacting materials' microhardness $H_{c,1}$ and $H_{c,2}$. The model was concluded to correlate well to the experimental data (2.23), but having an absolute error between 50-100%.

Yovanovich, 1982

Equation 2.23 was later recorrealted by Yovanovich [15] resulting in

$$h_c = 1.25 \frac{k_s m_s}{\sigma_s} \left(\frac{P}{H_c} \right)^{0.95} \quad (2.24)$$

The model is valid for $10^{-6} \leq P/H_c \leq 2.3 \cdot 10^{-2}$. In a reviewing article, Sridhar and Yovanovich [16] concluded that Equation (2.24) agrees more closely with data from several earlier performed experiments, compared to a number of other selected theoretical elastic and plastic models.

Tien, 1968

Tien established another formula similar to Equation (2.23) but with different constants [17]. The variables of the formula was established using the Pi theorem, a method for nondimensionalization, and the values of the constants were derived from experimental data. The thermal contact conductance according to this model is given as

$$h_c = 0.55 \frac{k_s m_s}{\sigma_s} \left(\frac{P}{H_c} \right)^{0.85} \quad (2.25)$$

Tien acknowledges that the effect of flatness deviation is neglected in the model, and that the model is applicable for plates with no large scale flatness deviation [17].

Thomas and Probert, 1972

The following correlation has been suggested by Thomas and Probert [18], and is given in the European Space Agency's recommendations in 1989 [9]. This model requires knowledge of contact pressure, thermal conductivity, surface hardness and RMS roughness of the materials. The relationship for thermal contact conductance is given as

$$\log \frac{h_c A}{\sigma k_s} = C \log \frac{PA}{\sigma^2 H} + D \quad (2.26)$$

where A is the contact area, $C = 0.720 \pm 0.044$ for aluminum and $C = 0.743 \pm 0.067$ for stainless steel, $D = 0.66 \pm 0.62$ for aluminum and $D = 2.26 \pm 0.88$ for stainless steel. Thomas and Probert did not specify the whether the surface hardness H in the proposed model corresponds to microhardness H_c or not.

Mikic, 1974

Mikic analytically derived several expressions for thermal contact conductance, considering the case of plastic or elastic deformation [10]. For the case of plastic deformation, using a geometrical model, the thermal contact conductance was derived as

$$h_c = 1.13 \frac{k_s m_s}{\sigma_s} \left(\frac{P}{H_c} \right)^{0.94} \quad (2.27)$$

Mikic notes that above expression is only slightly different from the one suggested earlier by Cooper, Mikic and Yovanovich [4]. Mikic further develops Equation (2.27) to account for the effects of plastic flow and elastic displacement, but states that Equation (2.27) is sufficient for practical load ranges.

European Space Agency, 2010

The European Space Agency gives recommendations for estimation of joint thermal conductance [19]. Typical joint materials with corresponding surface finish and contact pressure intervals are listed together with resulting thermal contact conductance. Table 2.1 presents recommended values for all aluminum materials covered.

The contact pressure is assumed to be constant over the entire joint contact area and is therefore calculated as

$$P = \frac{F}{A} \quad (2.28)$$

With a measured surface finish and a calculated contact pressure, the resulting contact conductance is chosen conservatively as the lowest value of suitable conductance interval in Table 2.1. Now, the total conductance can be calculated by multiplying the conductance with the total joint area,

$$C_1 = h_c A \quad (2.29)$$

The European Space Agency furthermore assumes a lateral conductance, C_2 , of 0.3 W/K [19]. The total conductance is therefore calculated as

$$C_{tot} = \frac{1}{\frac{1}{C_1} + \frac{1}{C_2}} \quad (2.30)$$

2.3.4 Relationship for Relative Contact Pressure

Many of the presented models includes the microhardness H_c , and a way of determining this is therefore necessary in order to use the formulas. One replacement of the microhardness that has been used in a number of correlations is the assumption that $H_c \approx 3S_U$ [14], where S_U is the tensile strength of the material. Another used approximation is that the microhardness instead can be replaced by the yield strength, according to $H_c \approx 3S_Y$ [17]. These estimations of the microhardness is however criticized as they usually lead to an underestimation of the true microhardness [14].

Song and Yovanovich [20] developed a formula expressing the relative pressure P/H_c as

$$\frac{P}{H_c} = \left[\frac{P}{1.62c_1(\sigma_s/\sigma_0m)c_2} \right]^{1/(1+0.071c_2)} \quad (2.31)$$

where $\sigma_0 = 1\mu\text{m}$, c_1 is the Vickers correlation coefficient and c_2 is Vickers size index. In order to determine c_1 and c_2 , a series of Vickers test should be performed. In a Vickers test, a force is applied resulting in a quadratic indentation mark on the specimen surface.

Table 2.1: Recommended contact conductance values for aluminum alloys depending on surface finish and contact pressure. Source: [19].

Material	Surface finish [μm]	Contact pressure [kPa]	Contact conductance [W/m ² K]
Aluminum 2024-T3	0.152-1.65	13.8-2.41	114-738
Aluminum 2024-T4	0.305	317-6719	664-34600
Aluminum 2024-T4	0.203-1.27	1.24-8531	1180-21400
Aluminum 2024-T6	0.207-1.52	67-7870	1560-3230
Aluminum 2024-T6	0.076-0.228	1.38-138	284-1830
Aluminum 2024-T6	0.381-343	138-6547	340-17000

The diagonal of the indentation mark, called indentation diagonal, is then measured. The Vickers microhardness H_V is calculated as [21]

$$H_V = \frac{1.854F}{d_V^2} \quad (2.32)$$

where d_V is the indentation diagonal and F is the applied load. The Vickers microhardness and the indentation diagonal are correlated according to [21]

$$H_V = c_1 \left(\frac{d_V}{d_0} \right)^{c_2} \quad (2.33)$$

with $d_0 = 1\mu\text{m}$. With a set of H_V and d_V values, the c_1 and c_2 coefficients can be estimated, and then Equation (2.31) can be used to substitute the relative pressure P/H_c into known variables. It should be noted that c_1 is temperature dependent while c_2 is not [21].

2.4 Bolted Joints

The previous section reviewed models for estimation of contact conductance. The necessity of contact pressure as an input parameter for estimating resulting contact conductance was clarified from all presented models. Most models have been developed or experimentally evaluated using a well-controlled pressure that has been constant over the whole contact area. For bolted joints however, the pressure distribution resulting from an applied axial force in the bolt is not constant over the whole joint area. Consequently, an analytical estimation of contact pressure or contact pressure distribution between two materials joined by bolts requires an additional sets of models.

Firstly, a model relating applied torque on the bolt to resulting force in the joint is necessary. Secondly, a model for how this force is distributed in the form of contact pressure around the bolt is necessary to analytically predict the resulting contact conductance. A review of available models is presented below.

2.4.1 Relationship between Tightening Torque and Bolt Axial Force

An established relationship between applied torque and joint tension for a threaded fastener [22] is given by

$$\tau_{tot} = F_{ax}(0.16P + 0.58\mu d_2 + \mu_b r_m) \quad (2.34)$$

where F_{ax} is the bolt axial force, P is the thread pitch, μ is the coefficient of friction in the threads, d_2 is the mean diameter, μ_b is the coefficient of friction between the bolt head and the surface of the component and r_m is the mean radius of the contact area under the head, given by

$$r_m = \frac{d_s + d_h}{4} \quad (2.35)$$

where d_s is the outer diameter of the bolt head and d_h is the hole diameter. Hence, the bolt axial force excited by a given torque can be expressed as

$$F_{ax} = \frac{\tau_{tot}}{0.16P + 0.58\mu d_2 + \mu_b r_m} \quad (2.36)$$

For a given torque and bolt, the only unknown parameter is the friction coefficient in the threads and between the bolt head and the component surface. These two coefficients are often assumed to be equal in practical problems. However, an error in the estimation of the friction coefficients has a significant influence on the resulting estimation of axial force. Currently, RUAG Space estimates their coefficients of friction to $\mu = \mu_b = 0.28$.

2.4.2 Relationship for Pressure Distribution in Bolted Joints

The pressure distribution in a bolted joint is an important factor for the resulting thermal contact conductance. Figure 2.3 illustrates the contact region in a bolted joint. As can be seen, the contact between the plates diminishes with radial distance from the bolt and the contact is only strong close to the bolt. It is difficult to practically measure the actual pressure distribution, and analytical models supported by empirical testing are lacking.

Fernlund developed an academically renowned, analytical model for the pressure distribution in bolted joints, described in several articles [23][24][25]. The model is based on a conical stress distribution extending from the bolt head, see Figure 2.4. The radius of the stress zone is given by

$$x = \frac{d_s}{2} + z \tan \alpha \quad (2.37)$$

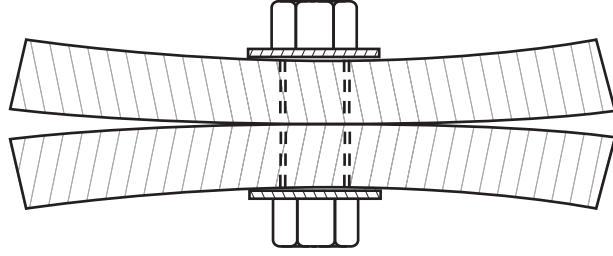


Figure 2.3: Contact of bolted joint.

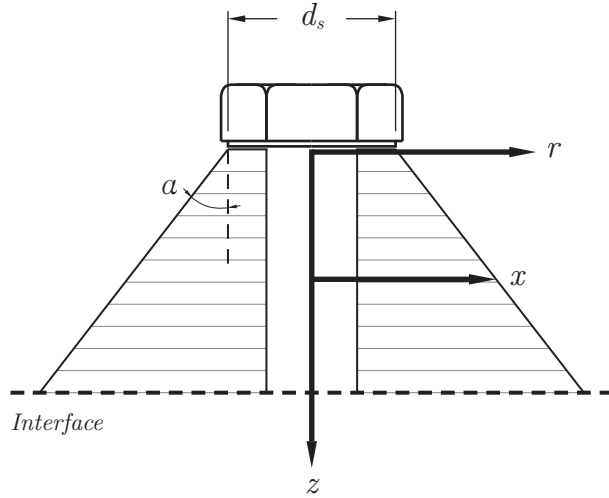


Figure 2.4: Pressure cone model.

where d_s is the diameter of the head in contact with the plate, z is the axial distance from the head and α is the angle of the cone, determining the lateral expansion of the stress zone. Outside the radius x , the stress is assumed to be zero. According to this model, the pressure can be determined as

$$P(r,z) = Ar^4 + Br^3 + Cr^3 + D + E \quad (2.38)$$

where P is the pressure between the two plates at radial distance r and axial distance z from bolt head. The variables $A-E$ are given by

$$A(z) = \frac{\frac{15}{\pi} \left(\frac{2}{d}\right)^6 F}{-\left(\frac{2x}{d}\right)^6 + 2\left(\frac{2x}{d}\right)^5 + 5\left(\frac{2x}{d}\right)^4 - 20\left(\frac{2x}{d}\right)^3 + 25\left(\frac{2x}{d}\right)^2 - 14\left(\frac{2x}{d}\right) + 3} \quad (2.39)$$

$$B(z) = -\frac{4}{3} \left(\frac{4x}{d} + 1\right) \frac{d}{2} A(z) \quad (2.40)$$

$$C(z) = \frac{4x}{d} \left(\frac{2x}{d} + 2 \right) \left(\frac{d}{2} \right)^2 A(z) \quad (2.41)$$

$$D(z) = -2x^2 d A(z) \quad (2.42)$$

$$E(z) = -\frac{1}{3} \left(\frac{2x}{d} \right)^3 \left(\frac{2x}{d} - 4 \right) \left(\frac{d}{2} \right)^4 A(z) \quad (2.43)$$

Hence, the required input for this model consists of the cone angle, α ; the axial joint force, F ; the axial distance from the head, z ; the bolt diameter, d and the diameter of the head, d_s . All of these are relatively easy to determine for a practical case except the cone angle, for which several values have been suggested over the years.

Examples of pressure distributions are presented in Figure 2.5, where the local pressure is given as a function of radial distance from the center axis of the bolt for three different bolt torques. The pressure curves have been calculated using Equation 2.36 to calculate the axial force, together with the Equations 2.37-2.43. The following parameters have been used: $P = 0.5$ mm, $\mu = \mu_b = 0.28$, $d_2 = 2.67$ mm and $r_m = 2.38$ mm in Equation 2.36; $d_s = 6.0$ mm, $z = 5$ mm and $\alpha = 40^\circ$ in Equation 2.37; $d = 3$ mm in Equations 2.39-2.43. The torques are $\tau = 0.8, 1.1$ and 1.4 Nm.

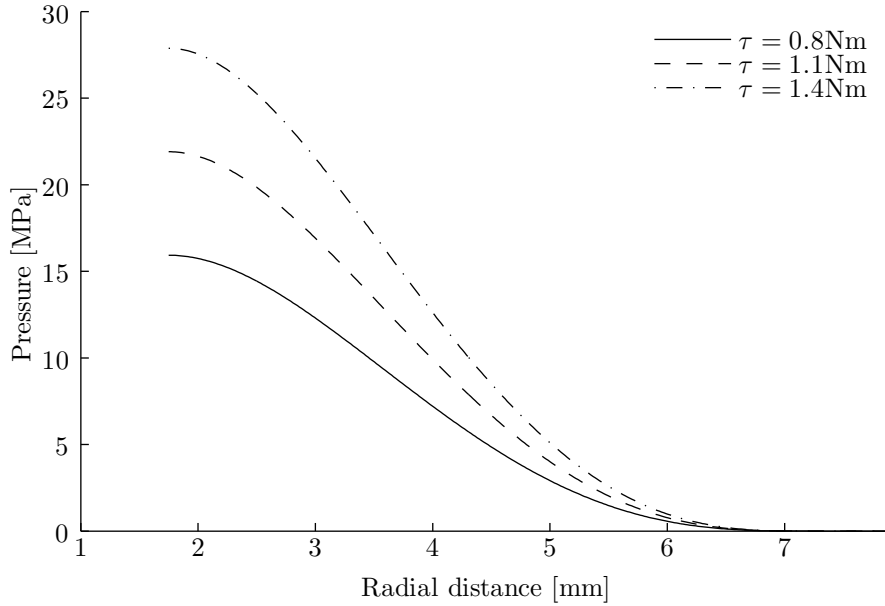


Figure 2.5: Illustration of pressure as a function of radial distance from bolt in a bolt interface. Three different torques, τ , are used.

2.5 Enhancement of Thermal Contact Conductance

The performance of the thermal conductance through a bolted interface are dependent on multiple factors. These factors are in principal all tied to the interface surface's protruding asperities, which determines the real contact area [26]. When aspiring increased thermal contact conductance, one or more of these factors may be refined, resulting in an increased area of contact, hence an increased thermal contact conductance.

The factors are generally acknowledged to be; applied joint pressure, surface roughness, surface flatness and thermal interface material [27].

2.5.1 Thermal Interface Material

An interstitial material can be placed between two clamped surfaces aimed at filling the natural gap formed due to the randomly distributed asperities on the interface surfaces [26]. The interstitial material is designed to deform and thereby adjust itself to the roughness of the surfaces. This will increase the real contact area of the clamped surfaces which in turn will increase the thermal contact conductance. On the left hand side in Figure 2.6, the contact situation without thermal interface material is illustrated, whilst the right hand side shows an idealized contact situation with thermal interface material, where the interstitial material completely fills the void.

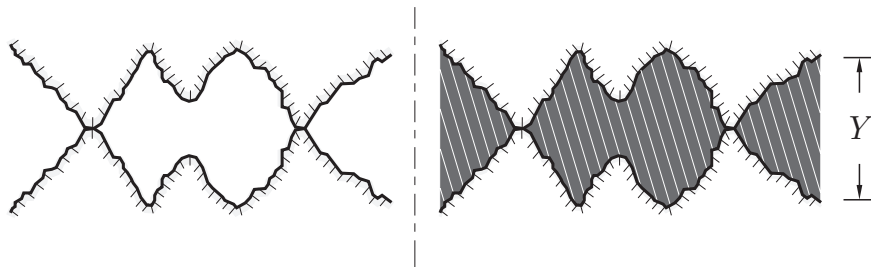


Figure 2.6: Illustration of ideal thermal interface material. Source: [26].

Ideally, a thermal interface material would have the following characteristics:

1. High thermal conductivity
2. Deform easily at low contact pressures
3. Minimal thickness
4. No leakage out of the interface
5. Maintaining performance indefinitely
6. Easy to assemble/disassemble

A lot of different interface materials are available on the market today, providing enhancement in thermal conductance. Unlike the idealized case where the interstitial material will completely fill the cavities, in reality there will still be gaps left, although less than without a thermal interface material. Also, the thickness of the interstitial material will be substantially larger than the idealized case, having a negative effect by its increase of thermal resistivity. This thickness, called the bond line thickness, is critical to minimize whilst at the same time being careful not to cause compromises to the filling of the whole surface [28]. Figure 2.7 illustrates the non-idealized contact situation of a thermal interface material. In vacuum conditions, an interstitial material will have a high influence

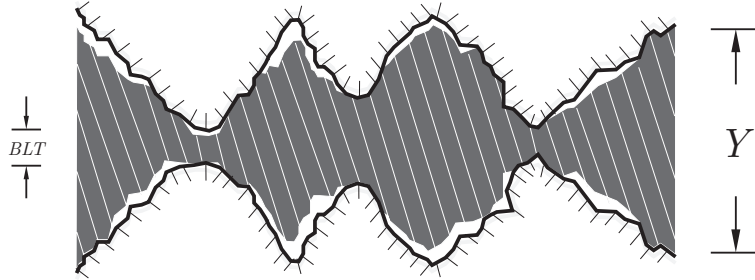


Figure 2.7: Illustration of real thermal interface material. Source: [26].

on thermal conductance due to the lack of otherwise present interstitial gas between the clamped surfaces. In the next sections, examples of the available categories in thermal interface material are presented.

Fluidic Materials

Thermal interface materials labeled as fluidic materials make use of their low viscosity to flow across the interface surface asperities when pressure is applied.

Thermal greases provide very low thermal resistance between reasonably flat surfaces [27]. They have the ability to completely fill the interface. The typical grease filler are based on polymeric matrix loaded with highly conducting filler particles. However, since they generally tend to migrate at low pressures and vaporize at high temperatures, they are not well suited for electronic systems [26]. Also, due to the wetness of these types of films, the need to remove and re-apply it is present for every dismantling of the interface.

PCM's, or phase change materials, which consist of high thermal conductivity particles and a base material, have the ability to flow like a thermal compound without migration and vaporization. Regardless of the name, these interstitial materials do not actually change phase but instead have their viscosity diminished when reaching a certain temperature, typically 50-90°C [26]. This allows them to further flow about the asperities to increase the contact area and hence, the contact conductance.

LMA, or liquid metal alloys, are naturally molten in room temperature which allows them to conform almost fully to the interface surfaces asperities. The melted state of the alloy and its conformity allows for very good contact conductance at a relatively

low contact pressure. These materials achieve the highest reduction in thermal resistance between the joint surfaces, next after soldering [28]. Although this high-flowing characteristic is optimal for minimizing thermal resistance in the joint, handling of it is challenging. Different measures have been taken to try and incorporate a gasket to contain the alloy or a filler to raise its viscosity, whilst still remaining its performance [29]. Liquid metal alloys most often contain gallium which is not compatible to use in aluminum joints. Gallium is corrosive to aluminum and will cause it to rapidly degrade.

Non-Fluidic Materials

There are several types of non-fluidic materials one might use to enhance thermal contact conductance in an interface.

Foils of soft metals, especially aluminum, copper, brass, gold, tin and indium, are a proven good thermal interface material [30]. Most commonly used and studied are aluminum, tin and indium foils. They provides moderate to excellent increase in joint thermal conductance, although at the cost of requirement of a relatively high contact pressure.

Polymeric fillers are usually classified into two classes, thermoplastics and elastomers. Due to their elastic deformation under strain and their viscoelastic behavior, thermoplastics and elastomers are a well-studied and common thermal interface material. Most often, highly conducting particles are added to the polymer to increase the thermal conductance performance [1][31].

Surface coatings might serve as an excellent substitute for grease and foils. Since it has wide spread usage it is also an acknowledged manufacturing principle and results can be well predicted. Results achieved in testing thermal contact conductance for aluminum specimens with indium, lead and tin coatings verified its effectiveness [32].

Carbon nanotubes has recently gained a lot of both industrial and academical focus, in the search for new and improved thermal interface materials [27][28]. These interstitial materials structures carbon nanotubes in a very dense array, perpendicular to the interface surfaces. When the joint is tightened, the carbon nanotubes create a connection between the interface surface's of the joint components.

2.5.2 Geometric and Application Optimization

In addition to usage of thermal interface materials, multiple geometrical and application properties of the joint can be modified, resulting in increased thermal contact conductance. In Section 2.2, factors influencing the thermal contact conductance were identified. By tuning these factors, one may increase the total contact conductance in the joint.

Contact Pressure

All analytical models expressing the thermal contact conductance mentioned in this thesis show heavy dependence upon contact pressure. According to these models, introduced in Section 2.3, increasing the contact pressure would enhance the thermal contact

conductance. This may be explained by a further elastic and/or plastic deformation of the asperities which results in an enlarged actual contact area and hence, a higher total thermal contact conductance. Figure 2.8 illustrates the effects of increased applied contact pressure.

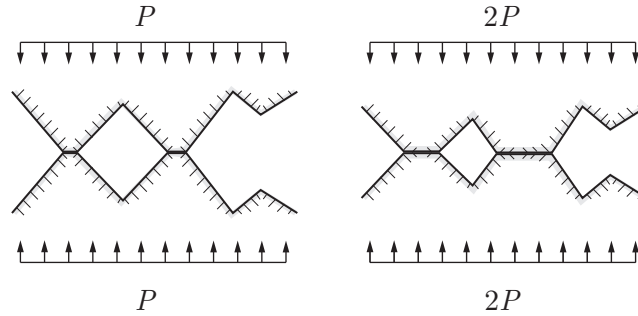


Figure 2.8: Effect of increased applied pressure on joint interface surfaces.

Surface Roughness and Flatness

By decreasing the surface roughness both the amplitude and sparsity of the asperities are reduced [33]. In turn, this will increase the real area of contact and reduce the height of the natural gap between the interface surfaces [12]. Both of these effects will contribute to a greater total thermal contact conductance.

Likewise for surface flatness, decreasing it will greatly and positively affect the total thermal contact conductance. Figure 2.9 illustrates effects of surface roughness and flatness optimization.

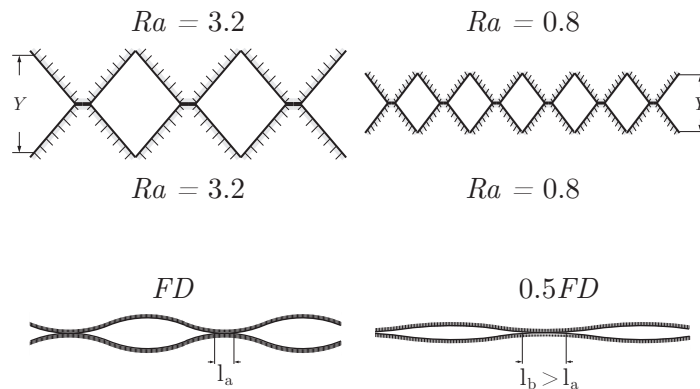


Figure 2.9: Effect of decreased surface roughness on joint interface surfaces.

Surface Hardness or Material Modulus of Elasticity

The softer the material or the lower the stiffness, the more its asperities will deform under the same applied joint pressure. When the surface asperities deform against each other, the real area of contact enlarges which, as previously explained, will increase the total contact conductance. Figure 2.10 illustrates this phenomenon.

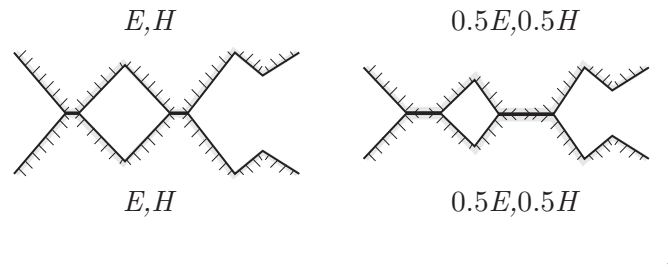


Figure 2.10: Effect of decreased material hardness or yield strength on joint interface surfaces.

2.6 Testing of Thermal Contact Conductance

The act of measuring thermal contact conductance is discussed in the following sections. Procedures of measurement on both cylindrical specimen as well as bolted joints are reviewed. Critique is given to measurement procedures of studied past research.

2.6.1 Cylinder Experiment

The general procedure to estimate the thermal contact conductance, h_c , for a certain set of material properties and experiment parameters is a cylinder test. This has previously been performed numerous times under slightly different circumstances. The basic approach is illustrated in Figure 2.11. Two thin cylinders with nominally flat contacting surfaces are pressed together and temperatures are measured at different distances from the contacting interface. The reason for using thin cylindrical specimens is to get a uniform heat flow through the interface. Also, as the cylinders are forced together, the interface will be exposed to a close to uniform pressure distribution. Schematically, the cylinder experiment make use of the following components [34][35][36][37]: a heater, inducing a known heat flow; a cooler, depositing the induced heat; thermocouples, measuring the temperature; and a radiation shield, minimizing radiation heat loss.

Since the pressure and heat flow is constant over the surface, so are also the thermal contact conductance and the temperature drop over the interface. Given the measured drop in temperature over the interface, the induced heat flow and the apparent area of contact, one can therefore calculate the thermal contact conductance, h_c according to Equation 2.5.

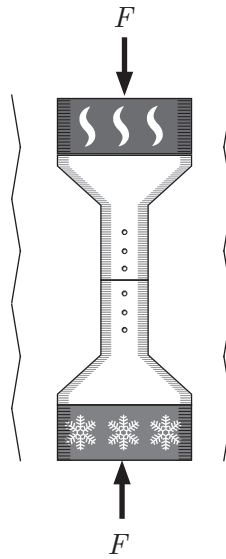


Figure 2.11: Schematic illustration of cylinder experiment.

2.6.2 Bolted Joint Experiment

A few published articles have tried to estimate the thermal contact conductance in a bolted joint, using somewhat different methodologies. Commonly their experimental setup consists of: a heater, inducing a known heat flow; a cooler, depositing the induced heat; thermocouples, measuring the temperature; a radiation shield, minimizing radiation heat loss; and a varying number of bolts. A schematic illustration of the general setup can be viewed in Figure 2.12.

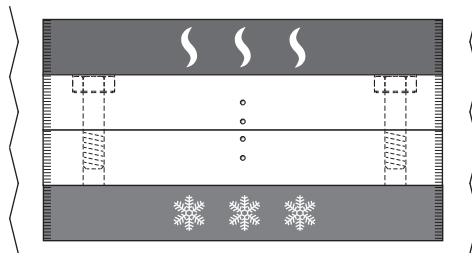


Figure 2.12: Schematic illustration of bolt joint experiment. A heater is placed on the top and a cooled base on the bottom. Thermocouples are positioned on both test specimens along a vertical line.

Sartre and Lallemand [38] and Yeh et al. [35] performed similar experimental measurements of thermal contact conductance in bolted joints. The temperature drop was determined using thermocouples positioned along one vertical line, surrounded by an

array of bolts, similar to Figure 2.12. The heat flow was estimated by calculating the temperature gradient from thermocouple readings, dT/dx , and by using Fourier's law given by Equation 2.1. These values were then used to estimate the thermal contact conductance according to Equation 2.5, and that result for was assumed as representative average for the whole joint interface.

Bevans et al. [39] applied another method of analysis for their experimental measurements on bolted joints. Several different perimeter bolt patterns were experimentally studied. Ten values of temperature drop over the interface were measured using pairs of thermocouples positioned close to the interface on each side of the interface. Different areas of the interface were divided into zones, depending on the distance to a certain bolt pattern. A representative temperature drop for the whole interface was calculated from the temperature drops of each zone, taking the relative area of each zone into account. An average thermal contact conductance, h_c , was then calculated using the representative temperature drop, the total heat input and the total interface area.

Critique of Previous Bolted Joint Experiments

The methodology used by Sartre and Lallemand [38] and Yeh et al. [35] assumes that both the heat flow and the interface temperature drop are close to constant across the interface. This is a strong simplification. As the bolts induce a non-uniform interface pressure, likewise will the thermal contact conductance be non-uniform according to all thermal contact conductance models presented in Section 2.3. The non-uniformity of thermal contact conductance consequently causes a high variance in the heat flow, q , across the interface. Most of the heat flow will pass through the interface close to a bolt where the thermal contact conductance is high, while further from the bolts the heat flow will be negligible. Figure 2.13 illustrates how the heat flow is concentrated to the area closest to the bolt when passing the interface. The variations in heat flow and thermal contact conductance will automatically influence the interface temperature drop according to Equation 2.5, and the temperature drop is therefore not necessarily constant across the interface.

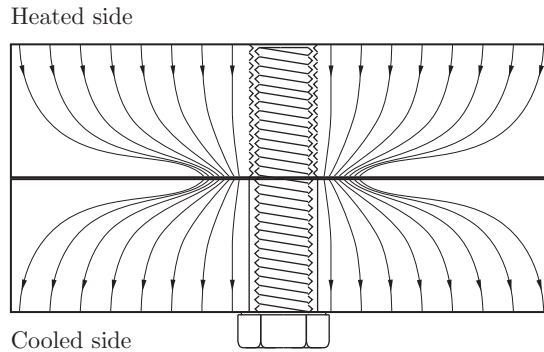


Figure 2.13: Heat flow in bolted joint.

Estimations of thermal contact conductance in bolted joints using one vertical array of thermocouples therefore give inaccurate results. The thermal contact conductance distribution of a bolted joint is difficult to determine and identification of a representative measurement position is extremely difficult. Sartre and Lallemand [38] and Yeh et al. [35] placed their thermocouples on the center axis of their specimen at the furthest horizontal distance from the bolts, and therefore most probably underestimated the average thermal contact conductance. The simplifications in this methodology are able to cause significant errors in estimation of thermal contact conductance.

The methodology used by Bevans et al. [39] assumes that a representative temperature drop can be found by simply averaging temperature drops, and that it can be used to calculate the average thermal contact conductance. There are however large areas where the thermal contact conductance is practically zero, and temperature measurements from these areas should not influence the thermal contact conductance. Since these areas are included, and the corresponding temperature drops are relatively high, the calculated thermal contact conductance will tend to be underestimated.

3

Method

This chapter describes the methodology of the experimental work. The experimental setup is reviewed in regards to its basic layout, procedures and equipment. Methods undergone to calculate unknown physical and material parameters are presented as well as the calculations executed on the resulting experimental data. The sources of error in regards to the experiments are discussed, evaluated and quantified. Actions taken during the experiments to minimize these errors are also presented. The evaluation and selection processes of tested thermal interface materials are described.

3.1 Layout of Experiments

The main focus of the conducted experiments was to determine empirical values of the thermal contact conductance in a joint, which later on were to be used as a reference for comparison with the found analytical models. The sought outcome of the experiments was the total thermal conductance, C_c , over the interface area of bolted joints as well as the relationship between thermal contact conductance, h_c , and interface pressure, P , of a generic joint. As the thermal contact conductance is dependent on numerous parameters, tests were conducted while varying these, in order to map possible dependencies.

A combination of two experiments constituted the basis for the empirical investigation. Firstly, a thermal contact conductance test was conducted using a generic interface of two thin cylinders with flat contacting surfaces. This thin, flat interface created a homogeneous pressure distribution, which allowed for a precise estimation of the relationship between thermal contact conductance, h_c , and applied pressure, P . The results from this experiment were used when correlating the correctness of the identified analytical models. Secondly, thermal contact conductance tests on a variety of bolted joint setups were performed. These experiments gave the thermal performance and its dependence on parameters that differed between the setups.

To increase the confidence in estimation of the interface pressure distribution in

the tested bolted joints, pressure indicating paper was used to map both the radial distribution and the amplitude of the interface pressure. These estimations were, as stated above, to be used when determining the total thermal contact conductance for the bolted joints.

3.1.1 Varied Parameters in Bolted Joint Experiment

As previously explained, the thermal contact conductance is dependent on various physical, geometric and material parameters. The following parameters were all deemed influential on thermal contact conductance of bolted joints in vacuum environment and were varied during testing. These parameters were also deemed practically testable and relevant to RUAG Space.

Number of bolts

The number of bolts in the joints were varied from one to three, all applied by the same values of torque. Information could then be extracted regarding the effect on thermal contact conductance by number of bolts. An earlier empirical study concluded that increasing the number of bolts in a joint increases the thermal contact conductance, even if the average contact pressure in the joint is kept constant [35].

Surface roughness

Reducing the surface roughness of the interface in a bolted joint increases the density of protruding asperities and the level of contact between the surfaces [12]. Earlier empirical studies have shown a correlation between finer surface roughness and increased thermal contact conductance [35]. Two surface roughnesses were tested in the experiments; normal and rough according to RUAG Space's manufacturing standards. The difference between these surface roughnesses was aimed to be significant enough to reveal the impact of surface roughness on thermal contact conductance. Due to difficulties in precisely acquiring a wanted surface finish when manufacturing, no specific values of surface roughness could be set except the requirement of $R_a < 0.8\mu\text{m}$ for the normal surface roughness.

Applied torque on bolts

The applied torque on the single bolt setup were set to 0.8, 1.1 and 1.4 Nm in selected experiments, in order to map the relationship between torque and thermal contact conductance. A higher torque increases the thermal contact conductance by causing a higher interface pressure.

Joint component materials

Three different material combinations were used in the empirical study: aluminum 6082 to aluminum 6082, aluminum 7075 to aluminum 7075 and aluminum 6082 to kovar. Material properties such as thermal conductivity and elasticity vary between materials and influences the thermal contact conductance. All aluminum specimens were nickel-plated and the kovar specimen was gold-plated. Relevant properties of these materials are given in Table 3.1.

Table 3.1: Properties for alloys/materials used for the test specimens.

Property	Al6082	Al7075	Kovar	Nickel	Gold
k [W/mK]	170	157	17.3	90.9	318
E [GPa]	68.6	72.0	138	200	79
α [$\mu\text{m}/\text{mK}$]	23.0	23.0	5.95-6.45	13.4	14.2
ν	0.33	0.33	0.312	0.31	0.44
S_U [MPa]	310	476	517	140-195	120

3.1.2 Varied Parameters in Cylinder Joint Experiment

The cylinder experiment was, as described in Section 3.1, conducted to investigate the relationship between thermal contact conductance and pressure. To achieve a high resolution curve on the effects of thermal contact conductance, h_c , versus applied pressure, P , six independent measurements were taken. The applied pressure was evenly distributed in the range of 2-25 MPa. The cylinder experiment was only performed for cylinders of aluminum 6082 with normal surface roughness, i.e. $R_a < 0.8\mu\text{m}$.

3.2 Setup of Experiments

This section covers the setup regarding chosen experiment equipment and test specimens of the bolted joint experiment as well as the cylinder experiment.

3.2.1 Bolted Joint Experiment

The test specimens chosen for the bolted joint experiments consisted of a rectangular top and bottom plate with a 84 mm by 40 mm contacting interface. The bottom and top plate incorporated three holes at a 28 mm equal distance. The bottom plate holes were countersunk 9 mm with a diameter of 6.5 mm and the matching holes on the top plate were fully threaded for M3 bolts. The bolts had a a spacing of 28 mm, in order to reduce overlapping of the pressure distribution. The protruding ledges of the bottom plate were used to clamp it to the bottom of the vacuum chamber. See Figure 3.1 for an exploded view of the bolted joint components. Four bottom plates were manufactured, each with a thickness of 12 mm. Two of these were aluminum 6082 with normal and rough surface roughness. The third bottom plate was aluminum 7075 with normal surface roughness. The fourth and last bottom plate had a different hole structure and was made in aluminum 6082 with normal surface roughness.

Five top plates were manufactured, three of them with a thickness of 5 mm, matching the first three bottom plates mentioned in choice of material and interface surface roughness. The fourth top plate matched the fourth and last bottom plate in choice of material and surface roughness but was only 3 mm thick. The fifth and last top plate

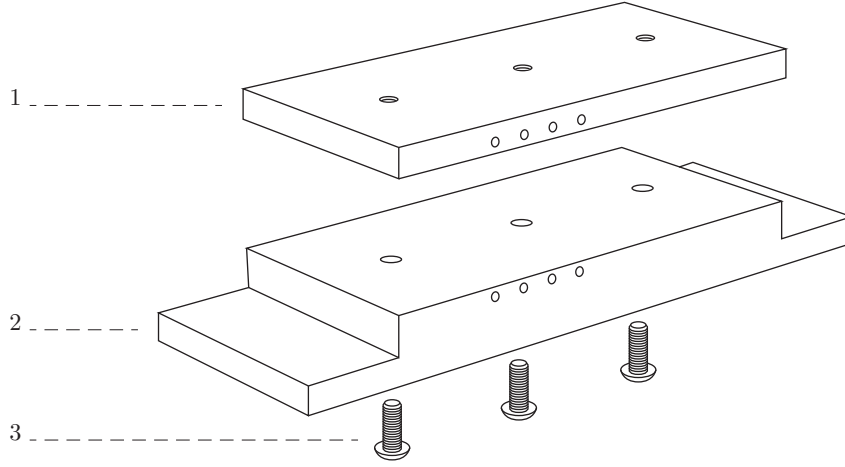


Figure 3.1: Illustration of bolted joint components. 1-Top plate, 2-Bottom plate, 3-Bolts.

Table 3.2: Configurations for the performed bolted joint experiments.

No.	Top mtrl	Bottom mtrl	Top/Bottom R_a	Top Thickness	Plating
1	Al6082	Al6082	Normal	5 mm	Nickel
2	Al6082	Al6082	Rough	5 mm	Nickel
3	Al6082	Al6082	Normal	3 mm	Nickel
4	Al7075	Al7075	Normal	5 mm	Nickel
5	Kovar	Al6082	Normal	4.5 mm	Gold
6	Filler 1	Filler 1	Normal	5 mm	Nickel
7	Filler 2	Filler 2	Normal	5 mm	Nickel

was made of kovar with normal surface roughness. It was used together with the first mentioned bottom plate.

All aluminum plates were nickel-plated, while the kovar plate was gold-plated. This was done in accordance with the standards of RUAG Space’s components and though it might affect the results, it was necessary in order to provide relevant results. The thickness of the platings was ordered to be $4 - 8\mu\text{m}$.

In total, experiments were performed on seven bolted joint configurations, see Table 3.2 for detailed configurations. The test specimens are illustrated assembled in Figure 3.2.

Configuration no.1 was a Al6082-Al6082 joint with normal interface surface roughness, tested with one bolt at 0.8, 1.1, 1.4 Nm of applied torque as well as with 2 and 3 bolts at a torque of 1.1 Nm. It was the most common type of joint present in RUAG Space’s

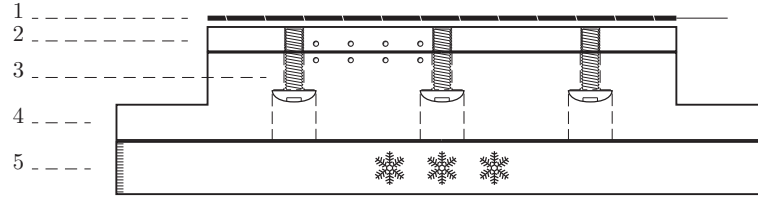


Figure 3.2: Illustration of experiment setup for bolted joint. 1-Heater, 2-Top plate, 3-M3 bolt, 4-Bottom plate, 5-Cooled base plate.

products.

Configuration no.2 was an Al6082-Al6082 joint with rough interface surface roughness, tested with one bolt for torques of 0.8, 1.1 and 1.4 Nm. This joint would illustrate eventual correlations between surface roughness and thermal contact conductance by comparing results with configuration no.1.

Configuration no.3 was a Al6082-Al6082 joint with normal interface surface roughness, tested with 1,2 and 3 bolts at 1.1 Nm torque. This configuration used the 3 mm top plate, representing another commonly present bolted joint in RUAG Space's products. Another difference in this joint was also the direction of the bolts, this time inserted from the top.

Configuration no.4 was a Al7075-Al7075 joint with normal interface surface roughness, tested with 1,2 and 3 bolts at 1.1 Nm torque. Aluminum 7075 has slightly different material parameters compared to aluminum 6082 and was to be introduced in RUAG Space's products.

Configuration no.5 was a kovar-Al6082 joint with normal interface surface roughness, tested with 1,2 and 3 bolts at 1.1 Nm torque. This type of joint was being used in certain products of RUAG Space.

Configuration no.6 shared the components from configuration no.1 and included the first tested thermal interface material. The joint was tested with one bolt for torques of 0.8, 1.1 and 1.4 Nm.

Configuration no.7 shared the components from configuration no.1 and included the second tested thermal interface material. The joint was tested with one bolt for torques of 0.8, 1.1 and 1.4 Nm.

Above configuration nomenclature is used throughout the rest of the report.

3.2.2 Cylinder Joint Experiment

The chosen test specimens consisted of two cylinders with a contacting interface of 10 mm in diameter. The small contact area allowed for relatively high and equal interface pressures, while using low loads. Away from the interface, both specimens had a conical shape with increasing diameter. This allowed for a lower interface pressure and a larger area for applying heat on the top specimen. Also these cylinders were plated with 4–8 μ m

nickel.

The two specimens were mounted in a test column together with a heater, two insulating glass fibre plates, two steel cylinders and a piezoelectric force sensor, see Figure 3.3.

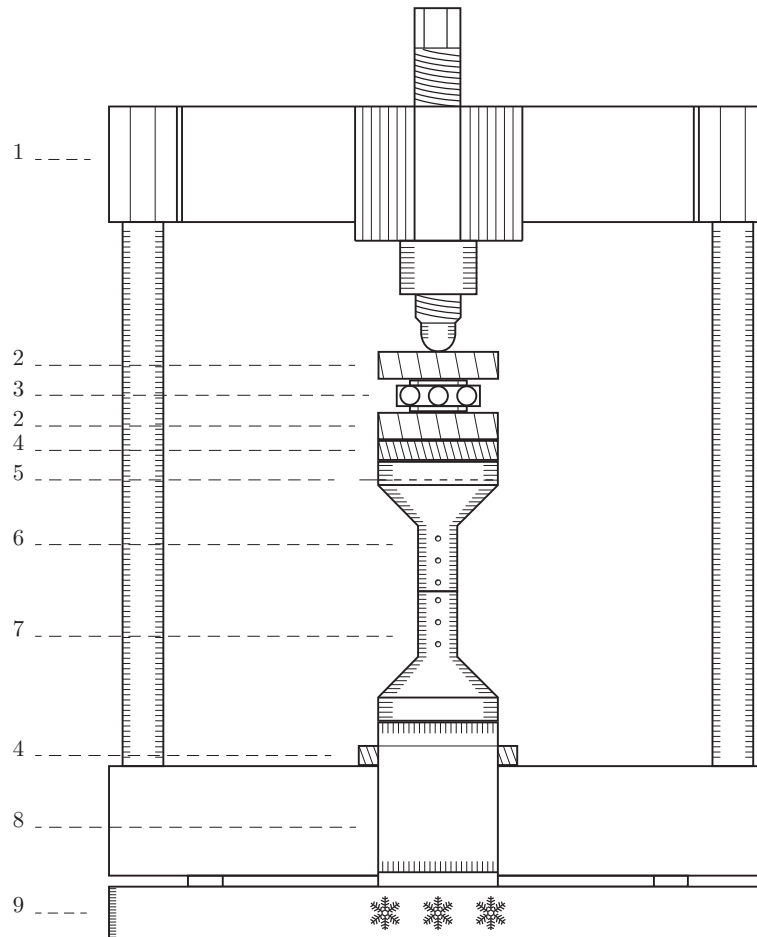


Figure 3.3: Illustration of experiment setup, cylinder. 1-Rig, 2-Spacer, 3-Force sensor, 4-Insulation, 5-Heater, 6-Top cylinder, 7-Bottom cylinder, 8-Aluminum plate, 9-Cooled base.

A load was applied in the axial direction of the column using a screw rig. The piezoelectric force sensor was used to measure the applied force on the column. The insulating cylinder on the top of the test column was used to prevent heat conduction away from the interface. Due to its large thermal mass, the screw rig was insulated from the heat flow with a bent aluminum plate, which led the heat flow down to the chamber base. Thereby, the time necessary to reach steady state of each test cycle was drastically shortened.

3.2.3 Placement of Thermocouples

For the bolted joint experiment, four holes with a diameter of 1.5 mm were drilled horizontally, as close as possible to the interface surface in both the top and bottom plates, see Figure 3.2. These holes enabled placement of the thermocouples in the center of the joints, equally spaced between two of the bolt holes. In total, eight thermocouples were mounted in each set of bolted joints, enabling measurement of the interface temperature drop ΔT at four separate locations.

For the cylinder joint experiment, three 1.5 mm holes were drilled perpendicular to the centerline in each of the two cylinders, which can be seen in Figure 3.3. The three holes were positioned at different distances from the interface and a thermocouple was mounted at the centerline in each hole. This enabled temperature measurement at different distances from the interface, enabling a calculation of the temperature gradient dT/dx in both specimens.

3.2.4 Equipment

All experiments were made in a vacuum chamber at a pressure of less than $1.0 \cdot 10^{-5}$ Pa.

The heaters used for the bolted joint experiments were 80 mm by 37 mm polyimide heaters. One heater was placed on the top surface of the each top plate, fastened by an adhesive layer. For the cylinder experiment a 20 mm by 30 mm polyimide heater was used. It was adhered on the top surface of the top cylinder in a milled countersink to prohibit direct contact with the upper structure.

Other equipment used during experiments were:

- Thermocouples class T
- 0-70V Power supply
- Hydra data processor
- Piezoelectric force sensor
- Fuji Prescale pressure sensitive film
- Torque wrench
- Equipment for surface roughness measurement
- Equipment for Vickers microhardness measurement

3.3 Procedure of Experiments

A similar procedure of experimental measurement was conducted for both the bolted joint and cylinder joint experiment:

1. A prepared bundle of thermocouples were bonded to the specimens with an epoxy. The readings of all thermocouples had been controlled and calibrated before test initiation.
2. For the bolted joint experiments, the bolt(s) in the joint were inserted and tightened according to the specifications of the test cycle. For the cylinder joint test, a specific axial force was applied.
3. The test specimen were clamped to the base plate of the vacuum chamber.
4. The thermocouples and heater cables were connected to the vacuum chamber connection module, as well as corresponding cables on the outside to the data processor and power supply.
5. Vacuum state was achieved and the base plate temperature stabilized at 0°C using the vacuum chambers heat exchanging system.
6. Specific amounts of power was applied on the heater in a sequence. The power input was changed after the system had reached steady state and the temperatures of the thermocouples had been read.
7. Normal pressure was achieved and a new test was initiated.

3.4 Estimation of Heat Losses

One of the main reasons for inaccuracy in vacuum measurements of thermal contact conductance is heat loss [34]. This opts for minimization and proper estimation of possible heat losses. Only heat losses occurring before the joint interface have been accounted for since losses after the interface do not influence the amount of heat passing through the interface. Discussed below are the identified sources of heat loss for the conducted experiments and the measures taken to minimize them.

3.4.1 Radiation Losses From Heater and Top Specimen

Radiation losses from heater and top specimen to the surroundings will occur as a consequence of temperature differences between the experimental setup and the walls of the vacuum chamber. The radiation heat flux to the chamber can be calculated as

$$Q_r = A_1 \sigma \epsilon_1 (T_1^4 - T_o^4) \quad (3.1)$$

where T_o and T_1 are the chamber and top specimen surface temperatures, ϵ_1 and A_1 are the emissivity and the surface area of the top specimen and σ is the Stefan-Boltzmann constant ($\sigma = 5.669 \cdot 10^{-8} \text{ W/m}^2\text{K}^4$). The emissivity of the nickel-plated specimens is low, $\epsilon \approx 0.03$, and causes a relatively low radiation. The heaters have a high emissivity, $\epsilon \approx 0.9$, and this together with its relatively high temperature could cause significant

radiation losses. The top surface of the heaters was therefore covered with aluminum tape, $\epsilon \approx 0.03$, decreasing the radiation loss with 97%, according to Equation (3.1).

If a radiation shield is deployed outside the experimental setup, the radiation heat flux to the shield becomes

$$Q_r = A_1 \sigma \frac{\epsilon_1 \epsilon_s}{(\epsilon_1 + \epsilon_2 - \epsilon_1 \epsilon_2)} (T_1^4 - T_s^4) \quad (3.2)$$

where T_s and ϵ_s are the temperature and the emissivity of the radiation shield. In order to further decrease the radiation losses, an aluminum foil was used as a radiation shield outside the experimental setup. Equation (3.2) was used to calculate the radiation from the test specimen to the shield and Equation (3.1) was used to calculate the radiation from the shield to the chamber. Assuming stationary conditions, these radiations are equal. Combining the equations and assuming the shield and test specimen to have the same surface area, the total radiation loss was given by

$$Q_r = \frac{A_1 \sigma \epsilon_1}{3 - \epsilon_1} (T_1^4 - T_o^4) \quad (3.3)$$

Above radiation corresponded to a further reduction of the radiation loss of 66%. A scenario analysis for the bolted joint experiment with $T_1 = 293\text{K}$, $T_o = 273\text{K}$, $\epsilon_1 = 0.03$ and $A_1 = 4.348\text{mm}^2$ gave $Q_r = 5 \cdot 10^{-3}\text{W}$. The use of aluminum tape and radiation shield was considered to result in negligible radiation loss for the bolted joint experiments, considering that all measurement had a heat input of 5.0 W or more.

In the cylinder experiment, the position of the heater inside the test column resulted in very little radiation loss to the surroundings. The heater was still covered with aluminum tape and the small radiation loss from heater and top specimen was neglected based on above analysis for the bolted joint experiment.

3.4.2 Conduction and Radiation Losses in Cables

Thermocouples and heaters will conduct heat from the test specimen to their connecting cables and heat will also be radiated from the cable surface to the chamber walls. Assuming constant temperature over the cross-section of the cable, the one dimensional heat conduction across the cable length is given by

$$q_c(x) = -k \frac{dT}{dx} \quad (3.4)$$

Type-T thermocouples consist of two insulated cables of copper and constantan, whose thermal conductivities at room temperature are $k_{cu} = 401\text{W/mK}$ and $k_{con} = 19.5\text{W/mK}$ respectively. The heaters were connected to the chamber wall connectors by four copper cables. These copper cables are, like the thermocouples, also insulated and has a thermal conductivity of $k_{cu} = 401\text{W/mK}$. The radiation from the plastic cover of the cable to the chamber walls is given by

$$q_r(x) = \sigma \epsilon (T(x)^4 - T_o^4) \quad (3.5)$$

where T_o is the chamber wall temperature. The emissivity of the plastic surfaces of the cables was assumed to be $\epsilon = 0.8$. The heat flow in a cable is schematically illustrated in Figure 3.4. With known temperatures at the cable ends, the temperature field and heat loss from specimen to cable can be solved numerically. In most of the performed tests, the top plate temperature was between 10-20°C and hence relatively close to the outside temperature of 20°C. A scenario analysis for four copper and constantan cables, and four copper cables connected to the heater, all of them with $T(0) = 293\text{K}$ (at the cable ends connected to the test specimen), $T(L) = 293\text{K}$ (at cable end connected to the outside), chamber temperature $T_o = 273\text{K}$, $L = 1.0\text{m}$, a copper diameter of $d = 0.5\text{mm}$ and an outer cable diameter of $d = 0.8\text{mm}$ gave a total heat loss of $Q_{tot} = 0.125\text{W}$. In order to minimize the losses, the thermocouple- and heater cables were covered with

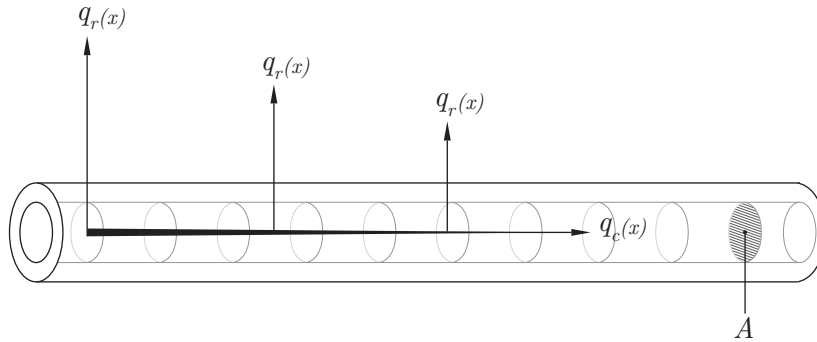


Figure 3.4: Heat loss in cable

MLI, lowering their emissivity to $\epsilon = 0.03$. This reduced the total heat loss of above scenario to negligible amounts.

3.4.3 Conduction Losses Through Insulation in Cylinder Experiment

The heat flow from the top cylinder to the force-controlling rig was minimized using insulation, see Figure 3.3. The insulation consisted of 8mm thick glass fibre plates. The thermal conductivity of the insulating plates and the thermal contact conductance in the contacting interfaces of the glass fibre plates were not fully known, and the the conductive heat flow was therefore unknown.

In the cylinder joint experiment, the total heat flow through the interface was estimated using Fourier’s law, where the three thermocouple readings from the top cylinder gave the temperature gradient. The heat loss from the top cylinder through the insulation did therefore not influence the estimation of heat flow through the interface, and an approximation of the heat loss was considered unnecessary. The estimation of the heat flow is described in section 3.6.2.

3.5 Measurement of Physical and Material Parameters

This section describes performed measurements of parameters whose quantitative values were uncertain. This includes measurements of the pressure distribution in the joint interfaces, the surface roughnesses of all mating surfaces and the microhardness for one specimen in the cylinder joint experiment. These measurements were performed in order to understand the physical conditions in the joint and to enable a comparison of mathematical models of thermal contact conductance with experimental results. Each measurement process is described below.

3.5.1 Pressure Distribution

A way of estimating the pressure distribution in the interface of a bolted joint analytically is described in Section 2.4.2. Since the available analytical models have a high degree of uncertainty, empirical determination of the pressure distribution was performed.

A thin pressure indicating film (product name Fujifilm Prescale[®]) was put in the interface of each of the tested bolted joints. The bolt(s) were tightened to the specific torque, released after 2 minutes, and the film was removed from the interface.

The pressure indicating film changed color and the intensity of the color corresponded to the level of experienced pressure. The used pressure indicating film had a pressure range of 2.5-10 MPa, Hence, pressure levels below 2.5 MPa gave no color change in the film, and pressure levels above 10 MPa gave a solid color of maximum intensity.

Based on the results of the pressure indicating films, the radius of the pressure zone around a bolt, r_0 , was estimated for each configuration. Figure 3.5 illustrates the process.

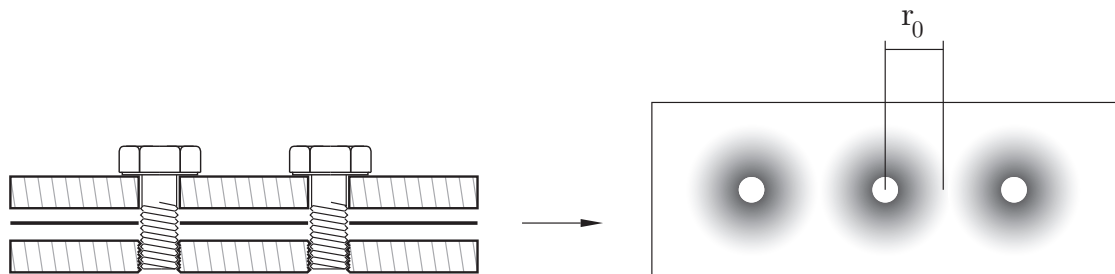


Figure 3.5: Illustration of the pressure distribution measurement.

3.5.2 Surface Roughness

Surface roughness was measured for the interface surfaces of all test specimens of the bolted joint and the cylinder experiment. A surface profiler using an optical interference microscope instrument was used for the measurements. Each surface was investigated at five different locations and the resulting values of surface roughness parameters R_a , σ and m were averaged. The results are given in Appendix E.

3.5.3 Microhardness

A Vickers hardness test was performed for one of the specimens of the cylinder test. This since the results of the cylinder test was used to evaluate analytical models where the microhardness was a necessary input. Four different loads were used; 0.05, 0.1, 0.2 and 0.5 kg. For each load, the Vickers hardness measurements was repeated three times. Resulting indentation diagonal, d_V and Vickers hardness, H_V , were obtained from the equipment and the three results were averaged. The results were assumed to be valid for the interface surfaces of both cylinder specimens, since they were manufactured in the same way from the same material. The results from the Vickers hardness test and the estimation of the variables c_1 and c_2 in Equation 2.31 are described in Appendix D. With estimated values of c_1 and c_2 , Equation 2.31 could be used to substitute the unknown value of H_c .

3.6 Estimation of Thermal Contact Conductance

This section describes the procedure of estimating the thermal contact conductance based on the experimental data. These calculations are described separately for the bolted joint and cylinder joint experiments below.

3.6.1 Bolted Joint Experiment

The total heat flow over the joint interface was estimated directly by the power input to the heater, since the heat losses was determined to be negligible in the bolted joint experiment, see Section 3.4. The power input was calculated through voltage and current readings from two voltmeters.

An initial numerical analysis showed a non-uniform temperature drop ΔT over an interface if applying a uniformly decreasing thermal contact conductance. This bore evidence of a non-uniform distribution of ΔT over the bolted joints, since the thermal contact conductance was expected to vary strongly across the interface. With varying interface temperature drop and thermal contact conductance, calculation of total contact conductance becomes a complicated and uncertain matter.

As discussed in Section 2.6.2, previously used methods for estimation of thermal contact conductance in bolted joints was considered to have limited accuracy. Therefore, a new method was developed in order to account for the complicated variations of thermal contact conductance.

The process developed in estimating the total thermal contact conductance of the tested bolted joints is illustrated in Figure 3.6. It uses an numerical processor that solves the 3-dimensional temperature field for a given contact conductance distribution. A cell centered finite volume method is applied to solve the temperature field in the bolted joint components. A theoretical description of this discretization method is found in [40]. The numerical processor can thereby return the temperatures in the positions of the thermocouples. This gives numerical values of the four temperature drops, ΔT_{num} ,

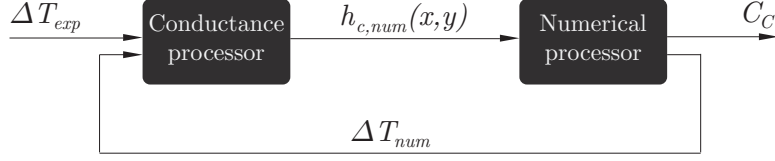


Figure 3.6: Process of total thermal contact conductance estimation.

for an assumed thermal contact conductance distribution. The process of determining the total thermal conductance is iterative and consists of four steps:

1. The four measured temperature drops, ΔT_{exp} , are fed into the conductance processor where they are stored as reference.
2. The conductance processor makes an initial guess of the distribution of thermal contact conductance over the bolted joint interface, $h_{c,num}(x,y)$.
3. The guessed contact conductance distribution, together with the boundary conditions and loads of the experiment, are used to numerically solve the 3-dimensional temperature field of the bolted joint. The numerical processor then returns four temperature drops, ΔT_{num} , calculated using temperatures at the thermocouple positions.
4. The numerical temperature drops are then compared with the experimentally measured ones, and the resulting difference is used to correct the thermal contact conductance distribution. This correction is then applied to the previous guess of the thermal contact conductance distribution, $h_{c,num}(x,y)$ and the process is restarted. The process is repeated until the temperature drop errors are below a certain limit.

The thermal contact conductance distribution was assumed to be axisymmetric around the bolt holes, diminishing linearly from a maximal value $h_{c,max}$ at the bolt hole radius r_h , down to zero at an estimated radial distance r_o . The heat transfer through the bolt was neglected because of the low conductivity of stainless steel ($k \approx 16$ W/mK) and the fact that heat transfer through the bolt has to pass two interfaces from the top to bottom plate. These two factors causes a significantly higher thermal resistance of heat passing the bolt compared to heat passing directly through the interface. The value of r_o was estimated based on the measured pressure distribution using the pressure indicating films, see Section 3.5.1. For each iteration, the value of $h_{c,max}$ was corrected as a consequence of temperature drop differences between experimental and numerical results. The iterative correction process is illustrated in Figure 3.7.

The linear relationship between h_c and r was chosen to simplify the analysis and it was considered as a relatively close approximation to the true distribution around a bolt. From the resulting pressure curves in Figure 2.5, it was concluded that the pressure could be approximated as linearly diminishing with radial distance from the bolt. Most analytical models, including Equation 2.19, 2.23, 2.24 and 2.27, also predicts a close to

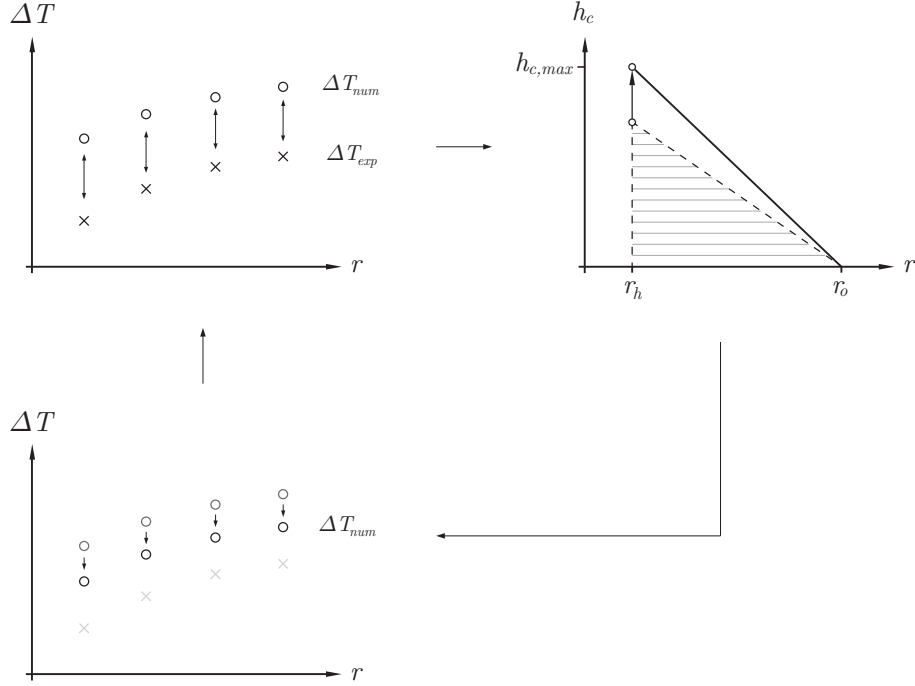


Figure 3.7: Illustration of the iterative optimization process.

linear relationship between pressure and contact conductance. Based on these observations, it was concluded that assuming a linear relationship between h_c and r resulted in a simple and sound model for the iterative process. When an optimal relationship between h_c and r was determined, the total thermal contact conductance could be calculated. This iterative process is described further with examples in Appendix C.

3.6.2 Cylinder Joint Experiment

The total heat flow over the joint interface was estimated by using the known thermal conductivity of the joint materials together with the temperature readings of the thermocouples of the top and bottom cylinders. A least squares line fit to the three measured temperatures of both cylinders gave the temperature gradients $\Delta T/\Delta x$. The average of the two temperature gradients was used since the gradients were considered to be relatively sensitive to possible errors in the thermocouples. The total heat flow could then be calculated using Fourier's law for one-dimensional flow, given by

$$Q_x = -kA \frac{\Delta T}{\Delta x} \quad (3.6)$$

Since the pressure distribution and all other parameters influencing thermal contact conductance could be considered constant over the interface, the contact conductance and interface temperature drop were also assumed to be constant. Extrapolation of

calculated temperature gradients for each cylinder specimen to the interface position gave an approximation of the temperature at each surface of the interface, whereby the temperature drop of the interface could be calculated. The thermal contact conductance was then given by

$$h_c = \frac{Q}{A\Delta T} \quad (3.7)$$

All measured values from the cylinder joint experiment are given in Appendix B.2. Figure 3.8 illustrates the estimation of the interface temperature gap, based on the six thermocouple readings.

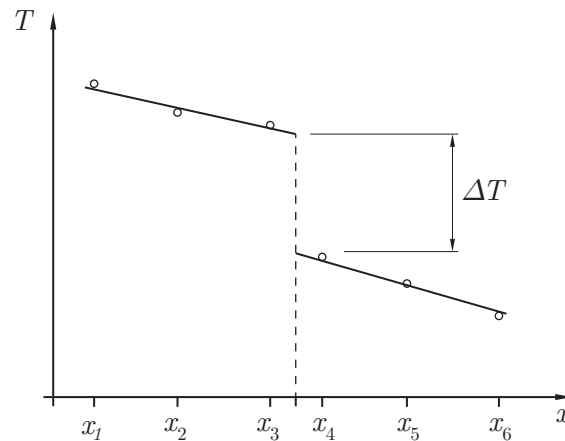


Figure 3.8: Illustration of temperature profiles for the estimation of interface temperature gap, based on six thermocouple readings.

The results from the cylinder experiment gave the correspondence between thermal contact conductance, h_c , and interface pressure, P .

3.7 Error analysis

This section describes identified sources of error of the performed thermal experiments in vacuum condition as well as their quantitative influence and measures taken to minimize them.

3.7.1 Uncertainty in Thermal Conductivity of Materials

The thermal conductivity of the test specimens is relatively well known, however a small amount of error in these values should be assumed. Also, the conductivity varies slightly with temperature, causing an increasing error as the temperature deviates much from reference temperatures.

3.7.2 Uncertainty in Heat Input in Bolted Joint Experiment

The heat input was controlled by the current through the heater. The voltage over the heater was measured by a separate voltmeter directly connected to the heater. This measurement system is called four-terminal sensing, illustrated in Figure 3.9, and allows for accurate calculation of voltage and current on the heater. The errors involved in this type of measurement are mainly the error marginal given by the voltmeter, which is $\pm 0.5\%$.

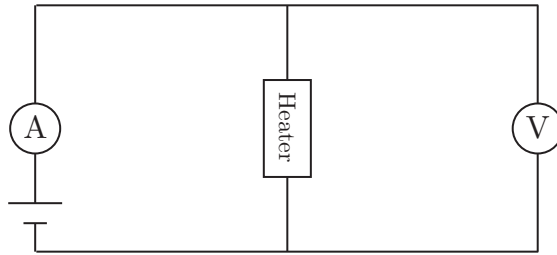


Figure 3.9: Illustration of four-terminal sensing.

3.7.3 Error in Thermocouples

Type-T thermocouples have an error of $\pm 0.5^\circ\text{C}$ and $\pm 1.0^\circ\text{C}$ in certain temperature ranges for class one and class two respectively. Due to this and due to the temperature range of the experimental applications, class one type-T thermocouples were used.

3.7.4 Uncertainty in Thermocouple Position

The uncertainty of the actual vertical position of the thermocouples are estimated to 0.5mm. This error comes from an uncertainty in the position of the drilled holes and the actual contact point of the thermocouple inside the hole.

3.8 Testing of Thermal Interface Material

With potential for great improvement in thermal contact conductance, two different thermal interface materials were tested, Keratherm Red 86/83 and T-pli 210. The goal of these tests was to empirically determine the increase in thermal contact conductance that could be achieved when using these thermal interface materials.

A range of different types of thermal interface materials was found from a selection of manufacturers. These were first individually evaluated with respect to basic compatibility requirements of RUAG Space.

The narrowed down selection of suitable thermal interface materials were then assessed and compared to a reference product, Cho-therm 1671, which was currently used by RUAG Space. By using a Pugh matrix, all important properties could be evaluated

for each individual thermal interface material against the reference. For further information about Pugh matrices, see [41]. When the evaluation process was complete, a total score could be calculated for each product, enabling a top selection to be identified. The completed Pugh-matrix is presented in Appendix A.

Keratherm Red 86/83 is a fibre glass reinforced silicone elastomer produced by Kerafol [42], and T-pli 210 is a boron nitride filled silicone elastomer produced by Laird Technologies [43]. Both of these thermal interface materials came in close agreement of the preferences set by RUAG Space. The thermal interface material was to be: space application compliant; highly thermal conductive; electrically insulating; easy to apply, remove and reuse; and well-performing in low pressure applications.

For results of thermal contact conductance improvement by the thermal interface materials, view Chapter 4.4.

4

Result

This chapter presents the results from the experiments conducted. Estimated total thermal contact conductance for the bolted joint and cylinder joint experiments are presented. Analytical models for thermal contact conductance are evaluated against the results from the cylinder joint experiment. The results from tests of thermal interface materials are also presented. A full conclusive discussion of the results is found in Chapter 5.

4.1 Pressure Distribution in Bolted Joints

This section presents the resulting pressure distributions in bolted joints from the tests with pressure indicating film. Figure 4.1 is a photocopy of the pressure indicating film after being subjected to configuration no.1, using one, two and three bolts at a bolt torque of 1.1 Nm. The pressure indicating film has a pressure range of 2.5-10 MPa. Local pressures below 2.5 MPa does not influence the film and pressures above 10 MPa results in a solid black color. As can be seen, the pressure decreases rapidly with radial distance from the bolt hole. Pressure above 10 MPa is clearly reached close to the hole. From the results in Figure 4.1, it was estimated that the pressure zone around the bolts had a radius of $r_o = 10$ mm for configuration no.1. This radius was used as input for the estimation of thermal contact conductance, described in Section 3.6.1. The estimated radius of the pressure zone contains a large amount of uncertainty since pressures below 2.5 MPa are not visible and the method of using pressure indicating films gave variations in results when tests were repeated.

Figure 4.2 gives resulting pressure distribution for configuration no.1, using one bolt and bolt torques of 0.8 Nm, 1.1 Nm and 1.4 Nm. As can be seen, the pressure increases significantly with increased torque, as expected from Figure 2.5.

Figure 4.3 gives resulting pressure distribution for configuration no.2, using one bolt and a bolt torque of 1.1 Nm. As can be seen, the pressure intensity follows ridges,

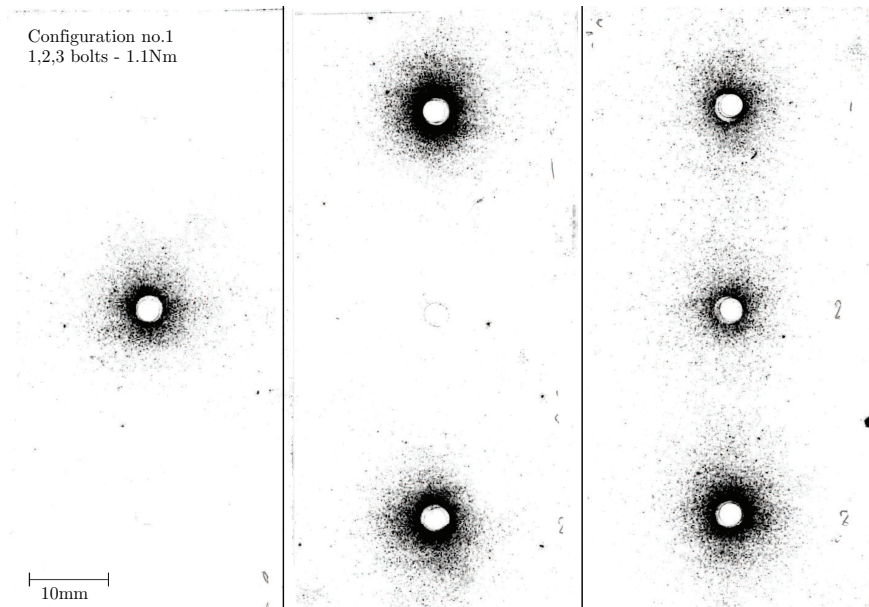


Figure 4.1: Resulting pressure distributions for configuration no.1. All bolts have been tightened with a torque of 1.1 Nm.

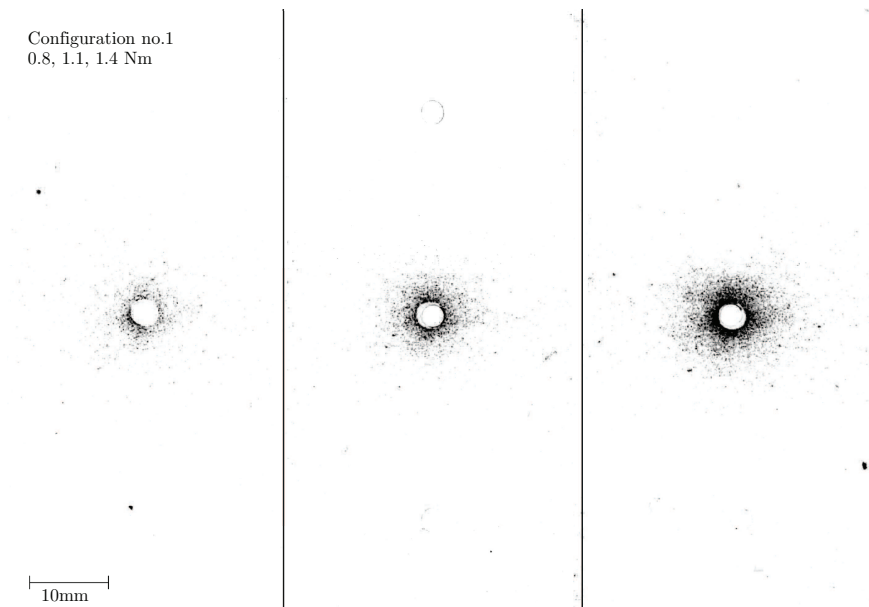


Figure 4.2: Resulting pressure distributions for configuration no.1. Applied torque are, from left to right; 0.8 Nm, 1.1 Nm and 1.4 Nm.

which were caused by the rougher manufacturing process. Also, pressure concentrations seem to exist on both edges of the interface. These effects complicates a determination of the size of the pressure zone. Therefore, it was estimated that the pressure zone around a bolt had a radius of $r_o = 20$ mm, to try to describe the irregular and extended pressure zone. The presence of pressure concentrations on the edges of the interface limited the reliability of the estimation of the total thermal contact conductance for this configuration.

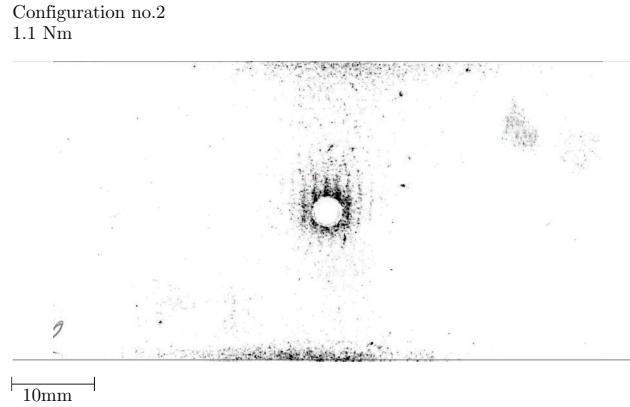


Figure 4.3: Resulting pressure distributions for configuration no.2, using one bolt and an applied torque of 1.1 Nm.

Figure 4.4 gives resulting pressure distribution for configuration no.3, using one, two and three bolts and a bolt torque of 1.1 Nm. Compared to Figure 4.1, this configuration has a pressure distribution strongly focused around the hole, with pressures above 10 MPa. Since the applied torque is 1.1 Nm here as well, both configurations should have the same total axial force and hence the same average pressure over the interface. This indicates that configuration no.3 has smaller pressure zones, and that the pressure distributions are concentrated to a close radius around the bolts. From the results in Figure 4.4, it was estimated that the pressure zone around a bolt had a radius of $r_o = 7$ mm for configuration no.3.

The difference between configuration no.1 and no.3 is no.3's thinner top plate and that it's bolts are positioned reversed, with the bolt heads on the top plate. A smaller distance from bolt head to interface gives a smaller pressure zone in the interface according to Equation 2.37 in Section 2.4.2, which explains the differences in pressure zone.

Figure 4.5 gives resulting pressure distribution for configuration no.4, using one, two and three bolts and a bolt torque of 1.1 Nm. Compared to the previous configurations, configuration no.4 has a pressure distribution that more widely extends from the bolt holes. For this configuration, it was estimated that the pressure zone around a bolt had a radius of $r_o = 12$ mm.

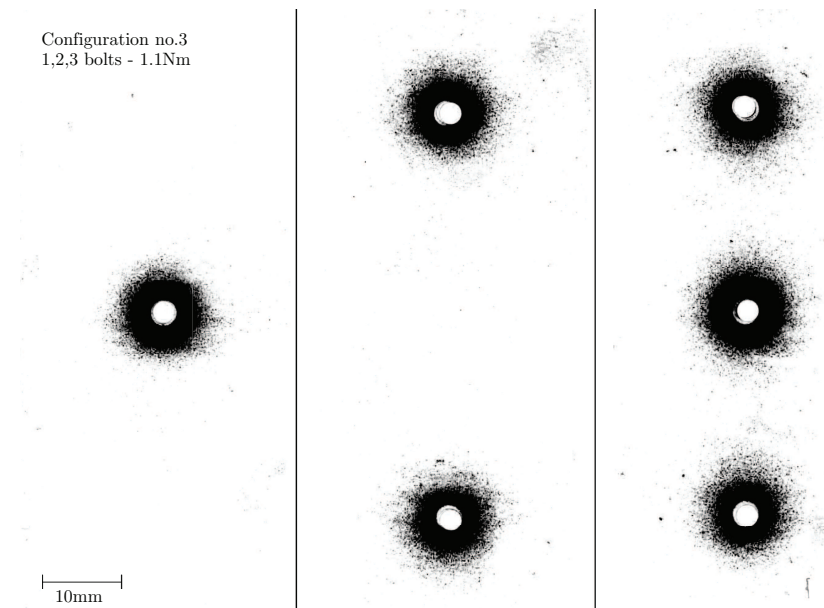


Figure 4.4: Resulting pressure distributions for configuration no.3. All bolts have a torque of 1.1 Nm.

For the case of two bolts in Figure 4.1 and 4.5, it can be seen that the pressure is not uniformly distributed around the bolt holes. Instead, the pressure zones extend further in the area closer to the short side edges.

Due to manufacturing errors, configuration no.5 were excluded from the results. The flatness deviation of the kovar top plate was not within acceptable limits and the joint gave unrealistic results out of both the pressure distribution experiment as well as the thermal contact conductance experiment. Configuration no.6 and no.7 used interface fillers, and no pressure tests were performed on these.

4.2 Thermal Contact Conductance

The following two sections present the resulting calculated thermal contact conductance for the bolted joint experiments and the cylinder joint experiments.

4.2.1 Bolted Joint Experiment

The resulting total thermal conductances from the bolted joint experiments are plotted in Figure 4.6 and Figure 4.7. They were derived using the iterative process previously explained in Section 3.6.1. The two figures plot the total thermal contact conductance of the joint interface against the two bolt parameters, bolt torque and number of bolts. Each one of the figures plot all joint configurations tested for varied bolt torque/number respectively.

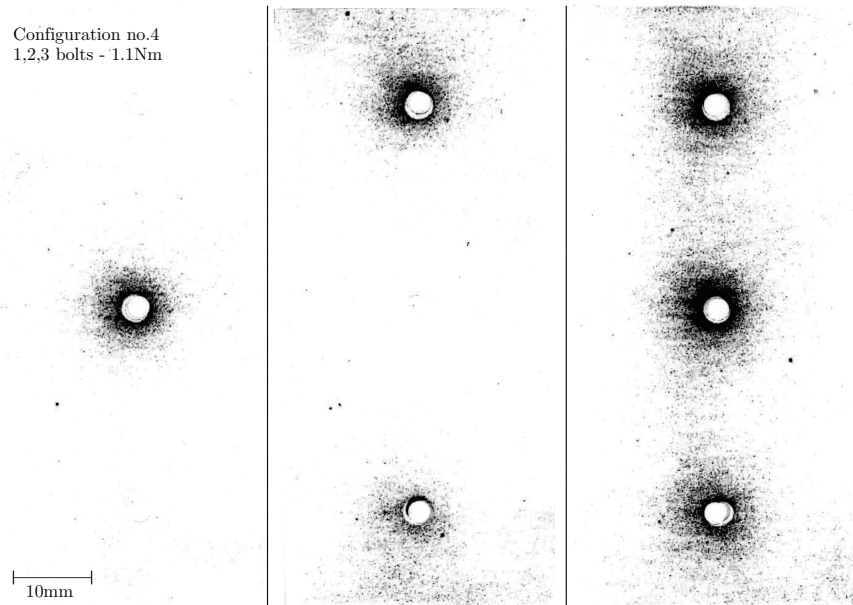


Figure 4.5: Resulting pressure distributions for configuration no.4. All bolts have a torque of 1.1 Nm.

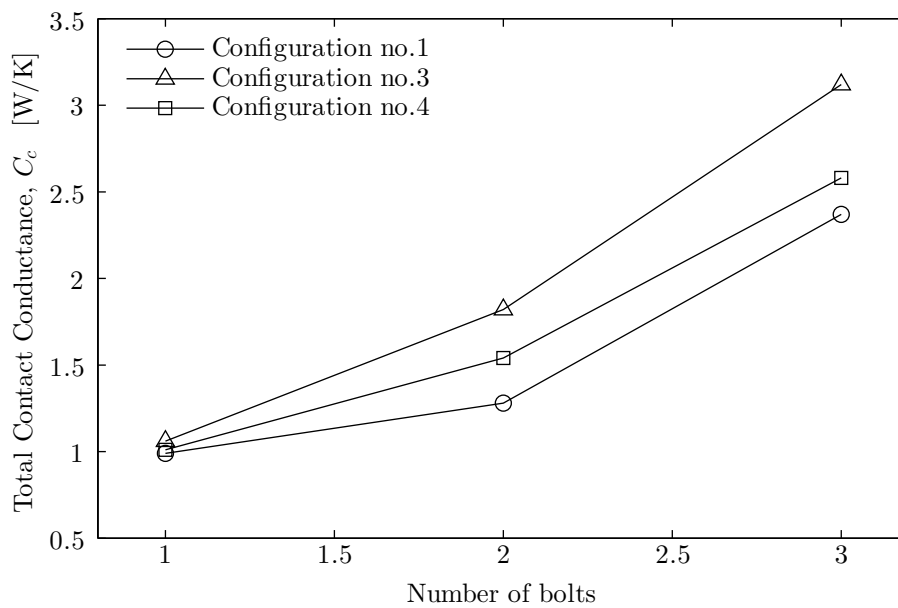


Figure 4.6: Resulting total thermal contact conductance in bolted joint experiment, with varying bolt number.

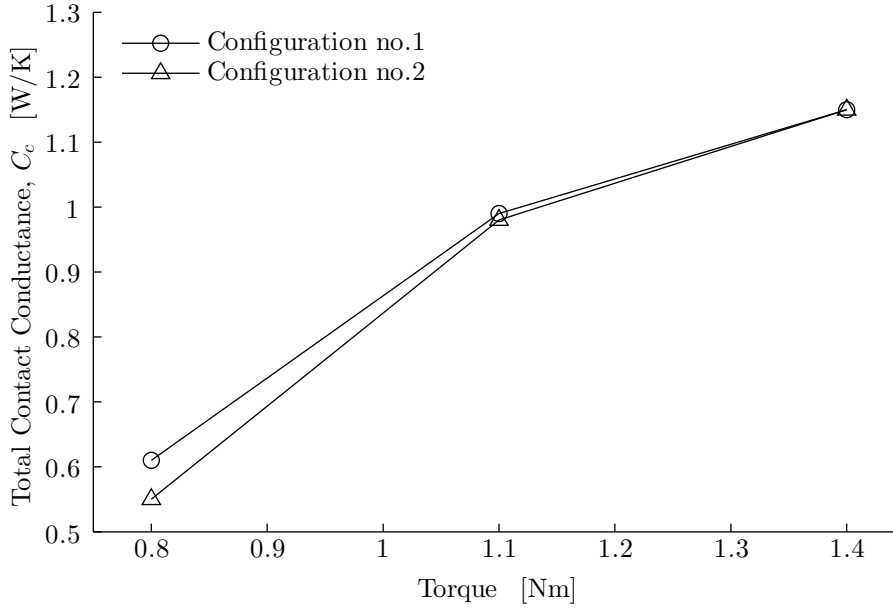


Figure 4.7: Resulting total thermal contact conductance in bolted joint experiment, with varying bolt torque.

As can be seen in Figure 4.6, both of the Al6082 configurations, no.1 and no.3, as well as the Al7075 configuration, no.4, perform close to equally when one bolt is applied. When a larger number of bolts is applied, configuration no.3 with its 3 mm top plate performs better than the two other configurations. According to the results, the Al7075 configuration, no.4, performs better than the Al6082 configuration, no.1. The results for configuration no.1 and no.4 show non-linearity of the increase in conductance relative to the increase in number of bolts. When applying two or three bolts in the joints the total thermal contact conductance is increased, as was expected, but not linearly. This means that an increase in bolts in the joint does not increase the total thermal contact conductance with the same factor, i.e. two bolts instead of one does not give two times the conductance.

These two characteristics of the results may be explained by mechanical influences of the bolts in the joint. Tension might occur due to horizontal clamping of the top plate when using two or three bolts. This may reduce the interface pressure achieved by the second and/or third bolt.

As can be seen in Figure 4.7, the total contact conductance is strongly increased with increased torque. The effect is however decreasing with a higher torque. The results in Figure 4.7 also indicate that configuration no.2, i.e. the Al6082 configuration with the rougher interface surface, performs worse for the tested torques. This result is in accordance with presented analytical models for thermal contact conductance in Section 2.3, which predicts decreasing h_c , and thereby decreasing C_c , with increasing R_a or σ .

However, because of the irregular pressure distribution in configuration no.2, shown by the pressure indicating film, low confidence in the results could be taken. This due to the need of a radial distribution of pressure around the bolts for the iterative method, used to calculate the total thermal contact conductance, to operate as intended.

4.2.2 Cylinder Joint Experiment

The result of the cylinder joint experiment is plotted in Figure 4.8. The thermal contact conductance were calculated in accordance with Section 3.6.2. The resulting thermal contact conductance is seen to increase with increased contact pressure, which is in conjunction with all identified theoretical models. The results also indicate a slightly parabolic relationship between pressure and thermal contact conductance.

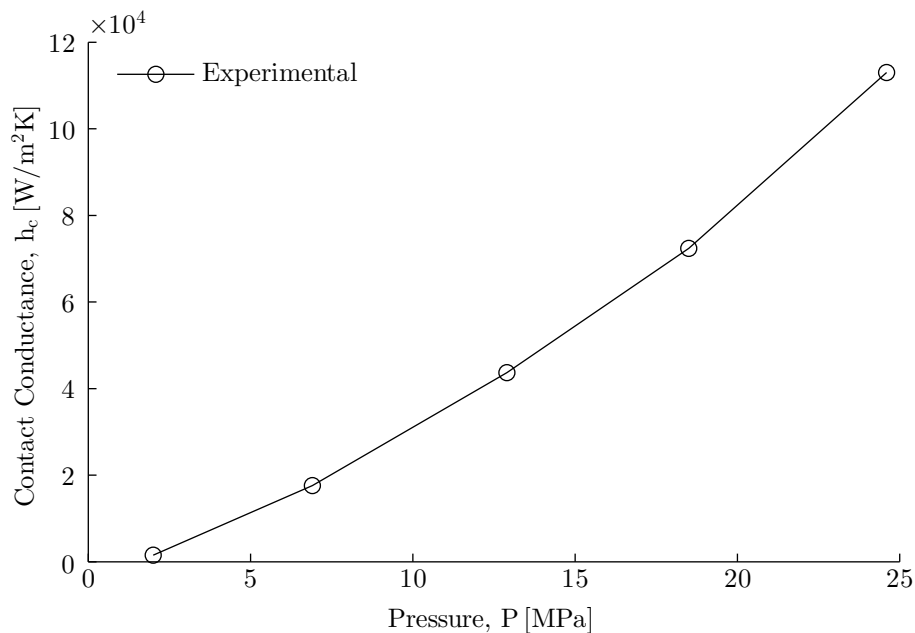


Figure 4.8: Resulting thermal contact conductance in cylinder joint experiments

4.3 Evaluation of Analytical Models

The identified analytical models were, as described in Section 3.6.2, evaluated through comparison with results of the cylinder joint experiment. The thermal contact conductance was calculated for each model, using parameters extracted from the experiment and measurements, for each applied pressure. The calculated thermal contact conductance from each analytical model plotted against the results of the empirical cylinder joint experiment can be seen in Figure 4.9. Material parameters for nickel, presented in

Table 3.1, were used in all analytical formulas for thermal contact conductance, since the surface layer consisted of nickel. All parameter values used for the calculation of the analytical models are given in Appendix F. The model by Thomas and Probert [18], was neglected since no explicit definition of hardness was given by the authors.

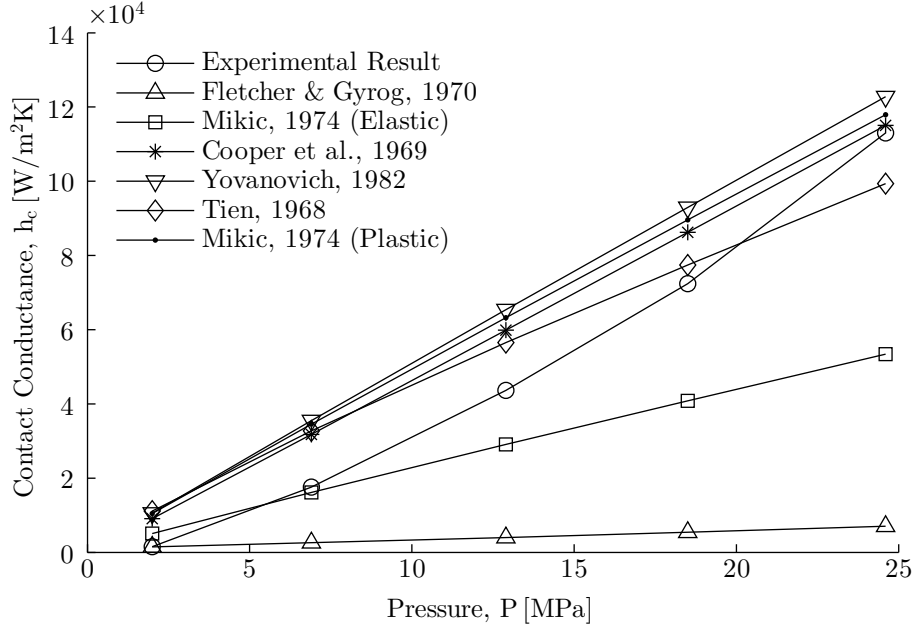


Figure 4.9: Experimental result compared with analytical models, where thermal contact conductance is given as a function of pressure. Corresponding analytical formulas are found in Section 2.3.

The analytical model in best accordance with the cylinder joint results is the Cooper et al. model [4]. As can be seen in Figure 4.9, it has the same overall trend although the absolute deviation is significant in most pressure ranges. A comparison plot of thermal contact conductance from the best found analytical model and the cylinder joint experiment can be seen in Figure 4.10.

4.4 Evaluation of Thermal Interface Material

The performance of the thermal interface materials were quantified by comparing the ratio of applied heat to average measured temperature drop, $Q/\Delta T_{avg}$ for the joint with and without the thermal interface material. In Table 4.1 and Table 4.2 the performance results are presented for T-ply 210 and Keratherm Red 86/83, respectively. The leftmost column describes the applied bolt torque, while column two and three describes the calculated $Q/\Delta T_{avg}$ values with and without the thermal interface material present. The rightmost column describes the estimated increase in thermal contact conductance

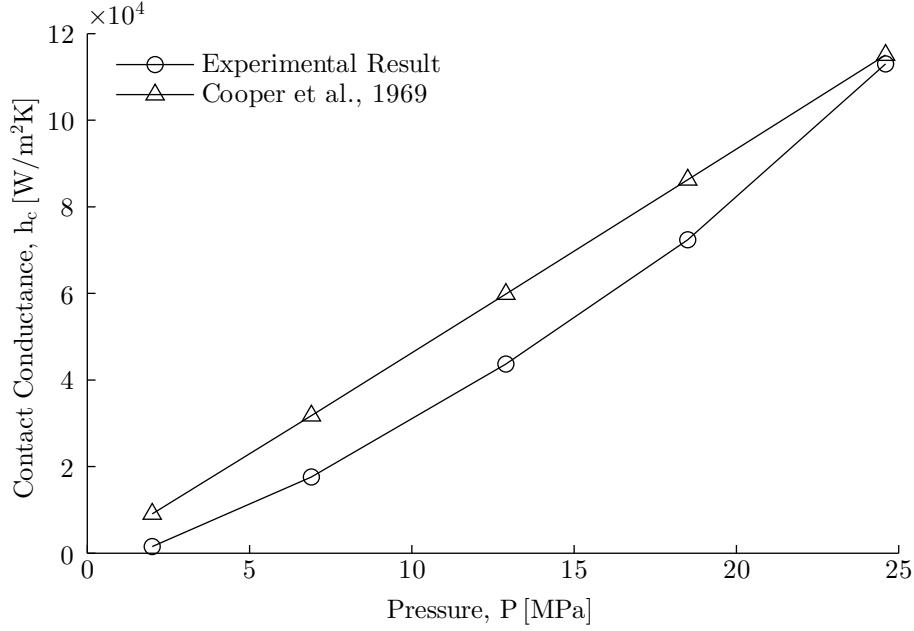


Figure 4.10: Experimental result compared with the Cooper et al. model, where thermal contact conductance is given as a function of pressure.

performance that was achieved when using the thermal interface material. All data from the experiments are presented in Appendix B.

In line with previous theory and with the results in 4.2.1, the $Q/\Delta T_{avg}$ ratio is seen to increase with increased bolt torque. This increase is seen both without the thermal interface material and with it. Comparing the $Q/\Delta T_{avg}$ ratios when using the thermal interface material to when not using it, a 24x-38x performance increase is seen for T-pli 210 and a 15x-23x performance increase for Keratherm Red 86/83. Similar for both thermal interface materials, a larger performance boost is present for lower bolt torques.

This method of estimating the thermal contact conductance has uncertainties in the results. It was used since the iterative method otherwise used was considered inappropriate in bolted joints with thermal interface materials.

Table 4.1: Evaluation of relative increase in average thermal contact conductance using thermal interface material T-pli 210.

Torque [Nm]	$Q/\Delta T_{avg}$ w/out TIM [W/K]	$Q/\Delta T_{avg}$ w/ TIM [W/K]	Increase
0.8	0.52	19.61	38x
1.1	0.79	20.75	26x
1.4	0.89	21.19	24x

Table 4.2: Evaluation of relative increase in average thermal contact conductance using thermal interface material Keratherm Red 86/83.

Torque [Nm]	$Q/\Delta T_{avg}$ w/out TIM [W/K]	$Q/\Delta T_{avg}$ w/ TIM [W/K]	Increase
0.8	0.52	12.12	23x
1.1	0.79	12.72	16x
1.4	0.89	13.41	15x

5

Conclusion

5.1 Pressure Distribution in Bolted Joints

Interface pressure in a bolted joint was found to vary strongly with radial distance from the bolt hole, decreasing at larger distances. Different configurations were found to have different distributions of pressure. The Al7075 bolted joint, configuration no.4, had a more extended pressure zone than Al6082, configuration no.1 and no.2. Configuration no.3, with the thinner top plate, had the most concentrated pressure zone.

The pressure indicating films gave slightly varying results for repeated tests and thereby the method was concluded to have some amount of uncertainty. However, by using the pressure indicating films, an approximate distance of the pressure zone could be estimated for the different bolted joints.

5.2 Bolted Joint Experiment

A new method for estimation of thermal contact conductance in bolted joints was developed. It combined empirically measured values of interface temperature drop with numerical simulations, in order to estimate the amplitude and distribution of thermal contact conductance more accurately than previous studies. Confidence in the method was strengthened by the good match between empirical input and simulation output.

Below follows conclusions regarding different parameters' effect on thermal contact conductance.

5.2.1 Number of Bolts

All tested bolted joint configurations had a total thermal contact conductance within the interval of 0.98-1.06 W/K when using one bolt at a bolt torque of 1.1 Nm. It is therefore concluded that a joint with one bolt gives a resulting total thermal contact conductance

of about 1 W/K for the tested materials and geometries. The same result should be expected for joints with a larger nominal contact area, i.e. larger top and bottom plates, since the pressure zones of all one-bolt configuration was determined to be contained within the boundaries of the tested joint size for one bolt. All tested configurations were nickel plated and the accompanying similarity in surface characteristics is considered to explain the similarity in thermal contact conductance performance.

When the number of bolts is increased, different configurations perform differently. Configuration no.3, with the thinner top plate and the bolt head applied on top, showed the best performance and was close to maintaining an added total thermal contact conductance of 1 W/K per added bolt. The most probable explanations for its higher performance are that the pressure zones of the bolts are less dependent on each other and that the pressure zones are focused on a smaller area around the bolt, due to the placement of the bolt head against the thinner of the two mating plates. The results from the cylinder experiment indicated exponentially higher thermal contact conductance with higher pressure. Therefore, a more focused pressure zone gives a higher total thermal contact conductance, due to higher average pressure.

For the two other configurations, no.1 and no.4., the increase in total thermal contact conductance did not correspond to the addition of bolts. Hence, a doubling of bolts does not give the same increase in total thermal contact conductance. However, when using two bolts the pressure distribution around the bolts was found to be non-symmetric. This might have caused an underestimation of the true thermal contact conductance for the case of two bolts.

5.2.2 Surface Roughness

Two configurations differed nominally only in surface roughness of the contacting surfaces. However, the pressure indicating film test showed that the rougher configuration no.2 had pressure concentrations along two of the edges of the interface, far from the bolt. This might have been caused by global waviness of one of the contacting surfaces. This limited the quality of the method used to estimate the total thermal contact conductance for the bolted joint, since a significant amount of the heat transfer was expected to occur in the area around the edges with high pressure. The confidence in the results of total thermal conductance for configuration no.2, presented in Figure 4.7, is therefore limited.

The results in themselves shows small tendencies toward a higher total thermal contact conductance for the configuration with lower surface roughness. As described above however, the quality of the results for configuration no.2 is not considered high enough to experimentally conclude the effects of surface roughness on total thermal contact conductance.

5.2.3 Applied Torque on Bolts

From the experiments it is concluded that the total thermal contact conductance is strongly increased with an increased bolt torque. The relative increase in total thermal

contact conductance is higher than the relative increase in torque when the torque is increased from 0.8 Nm to 1.1 Nm, see Figure 4.7. This is in line with the exponential increase of thermal contact conductance with higher pressure, found in the results of the cylinder experiment. The trend is however disrupted by the result from the maximum torque, 1.4 Nm. This result might be explained by a failure of the numerical method to fully account for the strong concentration of thermal contact conductance close to the bolt hole. Placement of thermocouples closer to the bolt hole would have increased the accuracy of the numerical method, since information of the interface temperature drop close to the bolt becomes increasingly important when the thermal contact conductance becomes very high in that region. Therefore, the total thermal contact conductance for the case of 1.4 Nm might be underestimated.

5.2.4 Joint Component Materials

Two different aluminum alloys were tested in the bolted joint experiments: Al6082 and Al7075. Both materials gave similar results for one bolt, whereas the Al7075 performed slightly better when two and three bolts were applied. However, the level of certainty in the used method is not deemed high enough to conclude that Al7075 performs better than Al6082.

5.2.5 Thermal Interface Material

As expected, both tested thermal interface materials, T-pli 210 and Keratherm Red 86/83, showed great improvement of thermal contact conductance in tested bolted joint. Both thermal interface materials fulfill the preferences set by RUAG Space for use in space applications and are therefore considered as candidates for use in future products.

5.3 Analytical Model Evaluation

The accordance of the analytical models to the empirically achieved results of thermal contact conductance in the cylinder joint experiment varied strongly among the models. The model of Cooper et al. [4] showed the highest overall accordance to experimental results.

Depending on application, a certain model can be several hundred percent off, in estimation of true thermal contact conductance. Therefore, it is strongly advised to perform practical experiments for each specific application, to avoid significant errors due to arbitrary choice of theoretical model.

Bibliography

- [1] I. Savija, J. Culham, M. Yovanovich, Review of thermal conductance models for joints incorporating enhancement materials, *Journal of Thermophysics and Heat Transfer* 17 (1) (2003) 43–52.
- [2] M. Mantelli, M. Yovanovich, *Spacecraft Thermal Control Handbook*, 2nd Edition, The Aerospace Press, El Segundo, California, 2002, Ch. Thermal Contact Resistance, pp. 599–638.
- [3] L. Fletcher, D. Gyorog, *Heat transfer and spacecraft thermal control*, Vol. 24, MIT Press, Cambridge, 1970, Ch. Prediction of Thermal Contact Conductance Between Similar Metal Surfaces, pp. 273–288.
- [4] M. Cooper, B. Mikic, M. Yovanovich, Thermal contact conductance, *International Journal of Heat and Mass Transfer* 12 (1969) 1517–1520.
- [5] V. Antonetti, T. White, R. Simmons, An approximate thermal contact conductance correlation, *Journal of Electronic Packaging* 115 (1) (1993) 131–134.
- [6] M. Lambert, L. Fletcher, Thermal contact conductance of spherical rough metals, *ASME Journal of Heat Transfer* 119 (4) (1997) 684–690.
- [7] L. Tanner, M. Fahoum, A study of the surface parameters of ground and lapped metal surfaces using specular and diffuse reflection of laser light, *Wear* 36 (1976) 299–316.
- [8] M. Bahrami, J. Culham, M. Yovanovich, G. Schneider, Review of thermal joint resistance models for nonconforming rough surfaces, *Applied Mechanical Reviews* 59 (1).
- [9] Thermal Control & Life Support Division European Space Agency, Noordwijk, *Spacecraft Thermal Control Design Data* (1989).
- [10] B. Mikic, Thermal contact conductance; theoretical considerations, *Int. Journal of Heat and Mass Transfer* 17 (2) (1974) 205–214.

BIBLIOGRAPHY

- [11] J. Greenwood, J. Williamson, Contact of nominally flat surfaces, Proceedings of the Royal Society of London. Series A, Mathematical and Physical Sciences 295 (1442) (1966) 300–319.
- [12] R. Onions, J. Archard, The contact of surfaces having a random structure, Journal of Physics, D: Applied Physics 6 (2) (1973) 289–304.
- [13] A. Bush, R. Gibson, T. Thomas, The elastic contact of a rough surface, Wear 35 (1975) 87–111.
- [14] M. Lambert, L. Fletcher, Review of models for thermal contact conductance, AIAA Journal of Thermophysics and Heat Transfer 11 (2) (1997) 129–140.
- [15] M. Yovanovich, Spacecraft radiative transfer and temperature control, Vol. 83, Progress in Astronautics and Aeronautics, AIAA, New York, 1982, Ch. Thermal Contact Correlation, pp. 83–95.
- [16] M. Sridhar, M. Yovanovich, Critical review of elastic and plastic thermal contact conductance models and comparison with experiment, Journal of Thermophysics and Heat Transfer 8 (4) (1993) 633–640.
- [17] C. Tien, A correlation for thermal contact conductance of nominally-flat surfaces in a vacuum, in: D. Flynn, B. Peavy (Eds.), Thermal Conductivity, Proceedings of the Seventh Conference, National Bureau of Standards Special Publication 302, 1968, pp. 755–759.
- [18] T. Thomas, S. Probert, Correlations for thermal contact conductance in vacuo, Journal of Heat Transfer 94-C (2) (1972) 276–281.
- [19] Requirements & Standards Division European Space Agency, Noordwijk, Space Engineering, Threaded Fasteners Handbook (2010).
- [20] S. Song, M. Yovanovich, Relative contact pressure: Dependence upon surface roughness and vickers microhardness, Journal of Thermophysics and Heat Transfer 2 (1) (1988) 43–47.
- [21] M. Yovanovich, Micro and macro hardness measurements, correlations, and contact models, in: Proceedings of the 44th AIAA Aerospace Sciences Meeting and Exhibit, no. 979, Reno, Nevada, USA, 2006.
- [22] M. Mägi, K. Melkersson, Lärobok i Maskinelement, EcoDev International, Göteborg, 2008.
- [23] I. Fernlund, A method to calculate the pressure between bolted or riveted plates, Tech. Rep. 17, Chalmers University of Technology, Gothenburg (1961).
- [24] N. Motosh, Determination of joint stiffness in bolted connections, ASME Journal of Engineering for Industry 98 (3) (1976) 858–861.

BIBLIOGRAPHY

- [25] S. Nassar, A. Abboud, An improved stiffness model for bolted joints, *Journal of Mechanical Design* 131 (12).
- [26] J. Gwinn, R. Webb, Performance and testing of thermal interface materials, *Microelectronics Journal* 34 (2003) 215–222.
- [27] F. Sarvar, D. Whalley, P. Conway, Thermal interface materials - a review of the state of the art, *Electronics Systemintegration Technology Conference* (2006) 1292–1302.
- [28] D. Saums, Developments with metallic thermal interface materials, <http://www.electronics-cooling.com/2007/05/developments-with-metallic-thermal-interface-materials/>, [Accessed 31 January 2012] (2007).
- [29] C. Macris, T. Sanderson, R. Ebel, C. Leyerle, Performance, reliability and approaches using a low melt alloy as a thermal interface material, http://enerdynesolutions.com/downloads/imaps_2004_man.pdf, [Accessed 31 January 2012] (2004).
- [30] S. Glasgow, K. Kittredge, Performance testing of thermal interface filler materials in a bolted aluminum interface under thermal/vacuum conditions, *Tech. Rep. NASA/TM-2003-212500*, NASA (2003).
- [31] R. Prasher, Thermal interface materials: Historical perspective, status, and future directions, in: *Proceedings of the IEEE*, Vol. 94, 2006, pp. 1571–1586.
- [32] T. Kang, G. Peterson, L. Fletcher, Effect of metallic coatings on the thermal contact conductance of turned surfaces, *Journal of Heat Transfer* 112 (4) (1990) 864–871.
- [33] K. Nishino, S. Yamashita, K. Torii, Thermal contact conductance under low applied load in a vacuum environment, *Experimental Thermal and Fluid Science* 10 (1995) 258–271.
- [34] C. Madhusudana, Accuracy in thermal contact conductance experiments - the effect of heat losses to the surroundings, *Int. Comm. Heat Mass Transfer* 27 (6) (2000) 877–891.
- [35] C. Yeh, C. Wen, Y. Chen, S. Yeh, C. Wu, An experimental investigation of thermal contact conductance across bolted joints, *Experimental Thermal and Fluid Science* 25 (2001) 349–357.
- [36] M. Sridhar, M. Yovanovich, Thermal contact conductance of tool steel and comparison model, *International Journal of Heat Mass Transfer* 39 (4) (1995) 831–839.
- [37] T. McWaid, E. Marschall, Thermal contact resistance across pressed metal contacts in a vacuum environment, *International Journal of Heat Mass Transfer* 35 (11) (1992) 2911–2920.

BIBLIOGRAPHY

- [38] V. Sartre, M. Lallemand, Enhancement of thermal contact conductance for electronic systems, *International Journal of Heat Mass Transfer* 35 (11) (1992) 2911–2920.
- [39] J. Bevans, I. Ishimoto, B. Loya, E. Luedke, Predictions of space vehicle thermal characteristics, Technical report, TRW Systems Group (1965).
- [40] J. Ferziger, M. Peric, *Computational Methods for Fluid Dynamics*, 3rd Edition, Springer, 2002.
- [41] P. Lindstedt, J. Burenius, *The Value Model: How to Master Product Development and Create Unrivalled Customer Value*, Nimba AB, 2003.
- [42] Kerafol, Keratherm[®]red data sheet, http://www.kerafol.com/fileadmin/user_upload/Thermalmanagement/downloads/englisch/datenblaetter/datenblaetter_2011/Keratherm_red.pdf, [Accessed 25 February 2012] (2012).
- [43] L. Technologies, T-ply 210[®] data sheet, <http://www.lairdtech.com/WorkArea/linkit.aspx?LinkIdentifier=id&ItemID=1921>, [Accessed 25 February 2012] (2012).

APPENDIX A

Selection of Thermal Interface Material

The selection of thermal interface materials to investigate was based on preferences set by RUAG Space. They expressed interest in a thermal interface material having the following properties

1. Compliant with ESA¹ rules for aerospace components
2. Excellent thermal conductivity
3. Electrically insulating
4. Easy to both apply, remove and reuse
5. Perform well under low pressure

Seven different thermal interface materials of different categories were found and assessed against a reference thermal interface material with similar properties. This reference product was Cho-therm 1671, already in use at RUAG Space. Table A.1 and A.2 shows the completed assessment in the form of Pugh matrices. As can be seen, T-ply 210, Keratherm Red 86/83 and Keratherm U90 were the highest rated among the thermal interface materials. Keratherm U90 was neglected from testing due to its similarities with Keratherm Red 86/83.

¹European Space Agency

APPENDIX A. SELECTION OF THERMAL INTERFACE MATERIAL

Table A.1: Pugh matrix 1/2, thermal interface materials

Requirement	Reference ChoTherm	Powerstrate Xtreme	Keratherm Red 86/83	Keratherm U90
Aerospace compliant	0	-	0	+
Thermal conductivity	0	+	+	+
Electrical insulativity	0	-	+	-
Apply/Remove	0	-	0	0
Needed pressure	0	+	+	+
Sum	0	-1	3	2

Table A.2: Pugh matrix 2/2, thermal interface materials

Requirement.	Reference ChoTherm	HiTherm 2505	Indium Coating	T-pi 210	Graphite S900
Aerospace compliant	0	0	0	+	0
Thermal conductivity	0	+	+	+	+
Electrical insulativity	0	-	-	0	-
Apply/Remove	0	-	-	0	-
Needed pressure	0	-	-	0	-
Sum	0	-2	-2	2	-2

APPENDIX B

Experiment Results

B.1 Bolted Joint Experiments

Tables B.1-B.7 present all measured data from the bolted joint experiments.

Table B.1: Experimental result data for configuration no.1; Al6082/Al6082, $R_a = 0.8\mu\text{m}$ and top plate thickness of 5 mm. Number of bolts, bolt torque, heater power and the four measured temperature drops are presented for each measurement.

No. of bolts	Torque [Nm]	P [W]	ΔT_1 [°C]	ΔT_2 [°C]	ΔT_3 [°C]	ΔT_4 [°C]
1	0.8	5.1	10.7	10.2	9.7	8.8
1	0.8	6.9	14.4	13.8	13.1	11.8
1	0.8	9.2	18.9	18.1	17.3	15.6
1	1.1	5.1	7.3	6.9	6.4	5.4
1	1.1	7.0	10.0	9.5	8.8	7.5
1	1.1	10.0	14.3	13.4	12.5	10.6
1	1.4	7.0	9.0	8.4	7.8	6.5
1	1.4	10.0	12.8	12.0	11.1	9.2
1	1.4	13.0	16.6	15.5	14.4	11.9
2	1.1	10.0	8.2	9.0	9.3	9.4
2	1.1	13.0	10.7	11.7	12.2	12.3
2	1.1	16.0	12.8	14.2	14.7	14.8
3	1.1	13.0	5.7	6.0	6.0	5.4
3	1.1	16.0	7.1	7.6	7.5	6.5
3	1.1	19.0	8.4	8.9	8.7	7.7

APPENDIX B. EXPERIMENT RESULTS

Table B.2: Experimental result data for configuration no.2; Al6082/Al6082, $R_a = 3.2\mu\text{m}$ and top plate thickness of 5 mm. Number of bolts, bolt torque, heater power and the four measured temperature drops are presented for each measurement.

No. of bolts	Torque [Nm]	P [W]	ΔT_1 [°C]	ΔT_2 [°C]	ΔT_3 [°C]	ΔT_4 [°C]
1	0.8	4.8	10.1	9.9	9.4	9.2
1	0.8	6.8	13.3	13.0	12.5	12.2
1	0.8	9.1	17.6	17.1	16.6	16.1
1	1.1	5.1	6.3	6.0	5.6	5.0
1	1.1	7.0	8.6	8.3	7.6	6.9
1	1.1	10.0	12.4	11.7	11.0	10.0
1	1.4	7.0	7.7	7.3	6.6	5.8
1	1.4	10.0	11.1	10.4	9.5	8.4
1	1.4	13.0	14.4	13.5	12.4	10.9

Table B.3: Experimental result data for configuration no.3; Al6082/Al6082, $R_a = 0.8\mu\text{m}$ and top plate thickness of 3 mm. Number of bolts, bolt torque, heater power and the four measured temperature drops are presented for each measurement.

No. of bolts	Torque [Nm]	P [W]	ΔT_1 [°C]	ΔT_2 [°C]	ΔT_3 [°C]	ΔT_4 [°C]
1	1.1	5.1	8.1	7.7	7.0	5.6
1	1.1	7.0	11.2	10.6	9.6	7.8
1	1.1	10.0	16.0	15.0	13.7	11.0
2	1.1	10.0	6.3	7.6	8.6	8.9
2	1.1	13.0	8.0	9.8	11.0	11.4
2	1.1	16.0	9.8	11.8	13.4	13.8
3	1.1	13.0	4.7	5.5	5.8	4.4
3	1.1	16.0	5.8	6.7	7.1	5.5
3	1.1	19.0	6.9	8.0	8.4	6.5

APPENDIX B. EXPERIMENT RESULTS

Table B.4: Experimental result data for configuration no.4; Al7075/Al7075, $R_a = 0.8\mu\text{m}$ and top plate thickness of 5 mm. Number of bolts, bolt torque, heater power and the four measured temperature drops are presented for each measurement.

No. of bolts	Torque [Nm]	P [W]	ΔT_1 [°C]	ΔT_2 [°C]	ΔT_3 [°C]	ΔT_4 [°C]
1	1.1	5.1	6.5	6.1	5.7	5.0
1	1.1	7.0	8.9	8.5	7.9	7.0
1	1.1	10.0	12.7	12.0	11.2	10.0
1	1.1	10.0	6.4	7.2	7.6	7.8
1	1.1	13.0	8.5	9.5	10.1	10.3
1	1.1	16.0	10.6	11.7	12.4	12.7
1	1.1	13.0	5.3	5.4	5.3	4.8
1	1.1	16.0	6.5	6.8	6.6	5.9
1	1.1	19.0	7.7	8.0	7.7	7.0

Table B.5: Experimental result data for configuration no.5; Kovar/Al6082, $R_a = 0.8\mu\text{m}$ and top plate thickness of 4.5 mm. Number of bolts, bolt torque, heater power and the four measured temperature drops are presented for each measurement.

No. of bolts	Torque [Nm]	P [W]	ΔT_1 [°C]	ΔT_2 [°C]	ΔT_3 [°C]	ΔT_4 [°C]
1	1.1	5.1	17.6	16.4	14.0	10.5
1	1.1	7.0	24.1	22.3	18.8	14.2
1	1.1	3.0	10.6	9.7	8.3	6.3
2	1.1	10.0	9.1	6.7	6.5	8.9
2	1.1	13.0	12.7	9.4	9.1	12.1
2	1.1	16.0	15.2	11.1	10.8	14.6

Table B.6: Experimental result data for configuration no.6; Al6082/Al6082 with filler T-Pli 210, $R_a = 0.8\mu\text{m}$ and top plate thickness of 5 mm. Number of bolts, bolt torque, heater power and the four measured temperature drops are presented for each measurement.

No. of bolts	Torque [Nm]	P [W]	ΔT_1 [°C]	ΔT_2 [°C]	ΔT_3 [°C]	ΔT_4 [°C]
1	0.8	19.0	1.7	1.0	0.8	0.7
1	0.8	25.0	2.0	1.2	1.0	0.9
1	0.8	55.1	4.6	2.8	2.3	1.7
1	1.1	25.0	2.1	1.3	1.1	0.9
1	1.1	55.0	4.2	2.6	2.1	1.7
1	1.4	25.0	1.9	1.2	1.0	0.8
1	1.4	55.1	4.1	2.5	2.1	1.7

Table B.7: Experimental result data for configuration no.7; Al6082/Al6082 with filler Keratherm Red 86/83, $R_a = 0.8\mu\text{m}$ and top plate thickness of 5 mm. Number of bolts, bolt torque, heater power and the four measured temperature drops are presented for each measurement.

No. of bolts	Torque [Nm]	P [W]	ΔT_1 [°C]	ΔT_2 [°C]	ΔT_3 [°C]	ΔT_4 [°C]
1	0.8	49.8	4.9	4.2	3.9	3.5
1	1.1	55.0	5.1	4.4	4.2	3.6
1	1.4	55.1	4.9	4.2	3.9	3.4

B.2 Cylinder Joint Experiments

Table B.8 presents all measured data for the cylinder joint experiment.

Table B.8: Experimental result data for the cylinder joint experiment, including interface pressure, electrical power input and temperature readings. The temperatures have been measured from thermocouples at the following distances from the interface: $x_1 = 16.5$ mm, $x_2 = 9.5$ mm, $x_3 = 2.5$ mm, $x_4 = -2.5$ mm, $x_5 = -9.5$ mm, $x_6 = -16.5$ mm.

P [Mpa]	Heat Flow [W]	T_1 [°C]	T_2 [°C]	T_3 [°C]	T_4 [°C]	T_5 [°C]	T_6 [°C]
2,0	0,9	15,3	14,7	14,2	6,6	6,2	5,8
6,9	2,6	18,4	16,7	15,4	12,5	11,1	9,9
12,9	5,0	28,8	25,9	23,3	20,1	17,5	15,5
18,5	7,3	39,2	35,1	31,2	27,4	23,6	20,7
24,6	7,1	37,5	33,4	29,7	26,4	22,7	19,8

APPENDIX C

Estimation of Total Thermal Conductance in Bolted Joint Experiments

This chapter will clarify the steps of the iterative process for determining total thermal contact conductance by using data and results from the experimental bolted joint configurations. This chapter will show data and analysis concerning configuration no.1, the aluminum 6082 joint with applied bolt torque of 1.1 Nm, using one, two or three bolts. All measurement data for these cases can be found in Table B.1.

Figure C.1 presents the experimental measurement of interface temperature drops for the case with one bolt with a torque of 1.1 Nm and a heat input of 10 W, together with interface temperature drop output from the final numerical simulation. The numerical output was derived using the thermal contact conductance distribution presented in Figure C.2. As can be seen, h_c is linearly decreasing from a maximum value closest to the bolt hole radius, $r_h = 1.75\text{mm}$, to zero at a radial distance from the bolt of $r_o = 10\text{mm}$. The estimations of r_o are given in Section 4.1. This h_c distribution was derived from the iterative process described in Section 3.6.1, and gave minimal interface temperature drop differences between the measured values from the experiment and the numerical simulation. As can be seen in Figure C.1, the experimental and numerical temperature drops are relatively similar, indicating that the numerical model gives an adequate approximation of the conducted experiment.

The total thermal contact conductance could then be determined as the sum of $Q/\Delta T$ for all interface faces in the numerical model, given by

$$C_c = \sum \frac{Q_i}{\Delta T_i} \quad (\text{C.1})$$

For a fine mesh (with a large amount interface faces) this becomes practically identical to the integral of the thermal contact conductance in Figure C.2, given by

$$C_c = \int_{r_h}^{r_o} 2\pi h_c(r)r dr \quad (\text{C.2})$$

Figure C.3 and C.4 presents the resulting interface temperature drops and thermal contact conductance distribution for two bolts. Figure C.5 and C.6 presents the resulting interface temperature drops and thermal contact conductance distribution for three bolts. Observe that the thermal contact conductance distributions are used around each bolt.

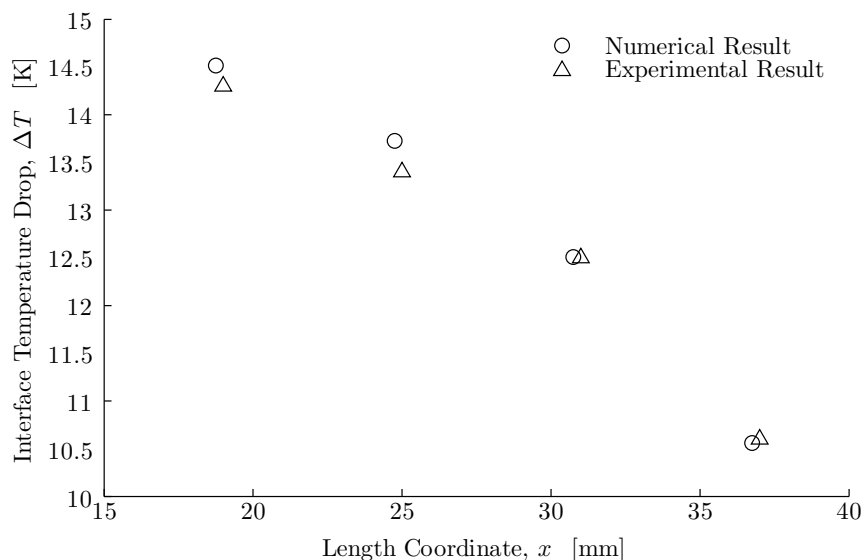


Figure C.1: Resulting interface temperature drop for both experimental measurements and numerical simulations, at given x-coordinates along the centerline of the interface. The experimental values are from configuration no. 1 with AL6082, $R_a = 0.8\mu\text{m}$, one bolt at $x = 42\text{mm}$ with 1.1 Nm applied torque, heat input of 10 W.

Figure C.7 presents the overall interface h_c distribution across the interface used in the numerical simulation for the case of three bolts. Figure C.8 presents the resulting interface temperature drop across the interface.

C.1 Cylinder Joint Experiment

Table C.1 displays the experimentally found thermal contact conductances for the applied contact pressures. Also, it displays the estimated thermal contact conductances given by the models presented in Section 2.3, using parameters emulating the cylinder joint setup.

APPENDIX C. ESTIMATION OF TOTAL THERMAL CONDUCTANCE IN BOLTED JOINT EXPERIMENTS

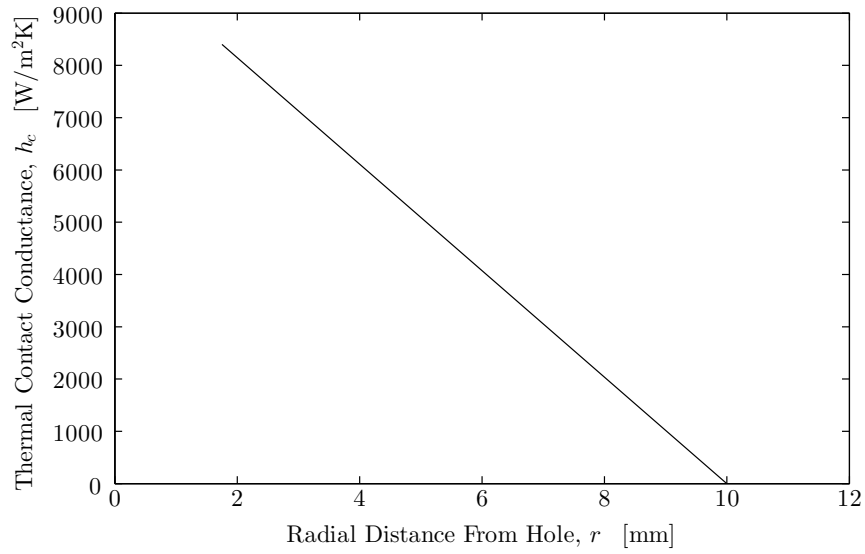


Figure C.2: Resulting thermal contact conductance as a function of radial distance from bolt, used in the numerical simulation for one bolt.

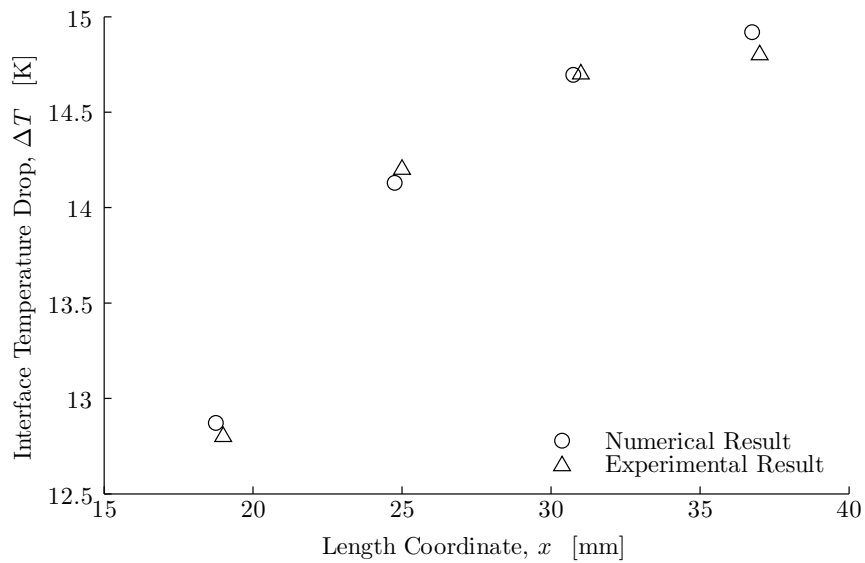


Figure C.3: Resulting interface temperature drop for both experimental measurements and numerical simulations, at given x -coordinates along the centerline of the interface. The experimental values are from configuration no. 1 with AL6082, $R_a = 0.8\mu\text{m}$, two bolts at $x = 42\text{mm}$ with 1.1 Nm applied torque, heat input of 10 W.

APPENDIX C. ESTIMATION OF TOTAL THERMAL CONDUCTANCE IN BOLTED JOINT EXPERIMENTS

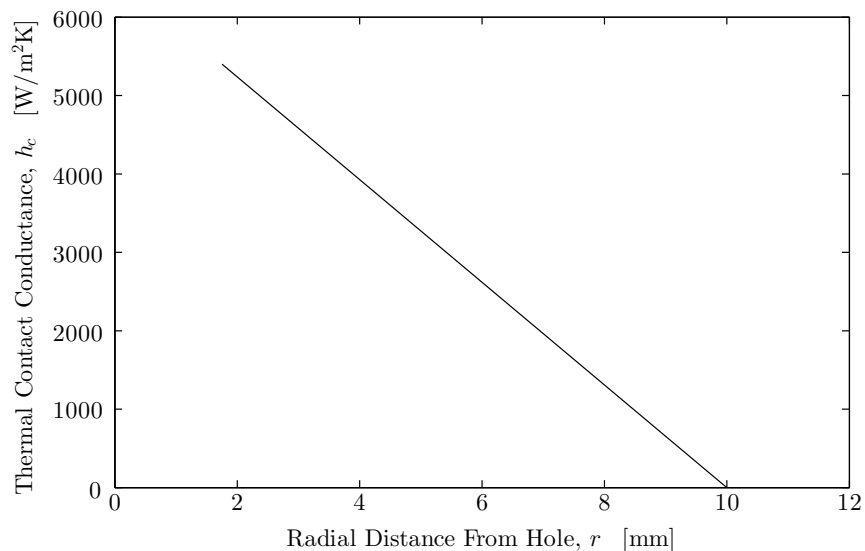


Figure C.4: Resulting thermal contact conductance as a function of radial distance from bolt, used in the numerical simulation for two bolts.

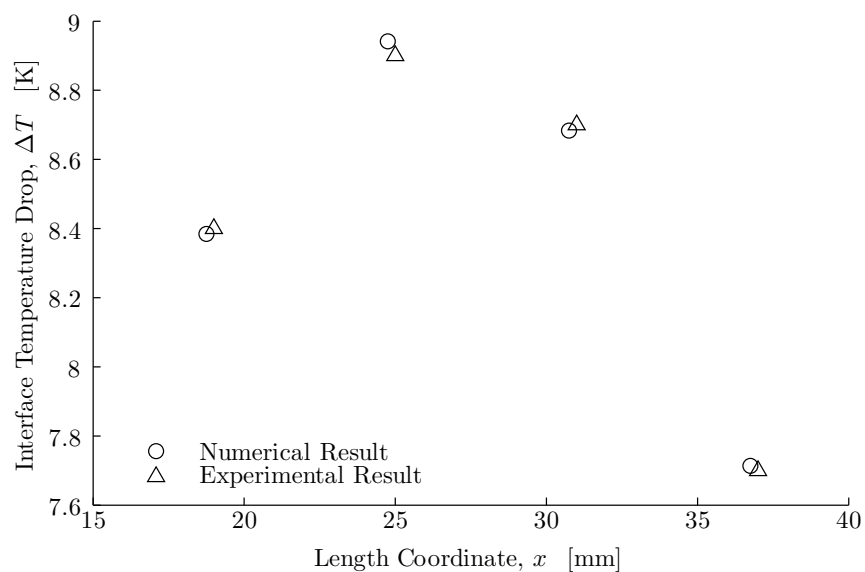


Figure C.5: Resulting interface temperature drop for both experimental measurements and numerical simulations, at given x -coordinates along the centerline of the interface. The experimental values are from configuration no. 1 with AL6082, $R_a = 0.8\mu\text{m}$, three bolts at $x = 42\text{mm}$ with 1.1 Nm applied torque, heat input of 19 W.

APPENDIX C. ESTIMATION OF TOTAL THERMAL CONDUCTANCE IN BOLTED JOINT EXPERIMENTS

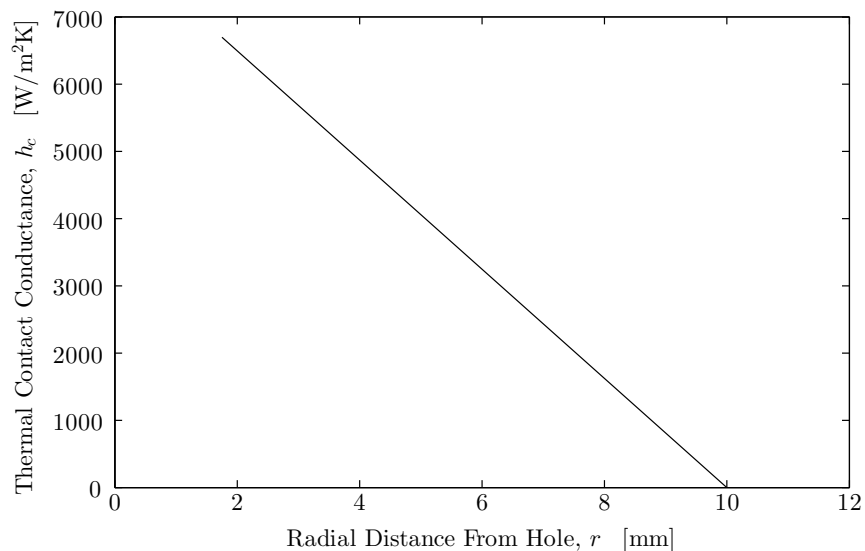


Figure C.6: Resulting thermal contact conductance as a function of radial distance from bolt, used in the numerical simulation for three bolts.

Table C.1: Experimentally and analytically estimated thermal contact conductance, h_c [W/m²K], for different contact pressures.

Pressure [Mpa]	2.0	6.9	12.9	18.5	24.6
Experiment	1509	17564	43654	72387	112994
Fletcher & Gyrog, 1970	1459	2619	4010	5444	7033
Mikic, 1974 (Plastic)	10449	34555	63234	89573	117953
Cooper et al, 1969	9077	31784	59872	86236	115064
Yovanovich, 1982	10599	35498	65380	92957	122767
Tien, 1968	11099	32731	56530	77451	99337
Mikic, 1974 (Elastic)	5045	16159	29097	40835	53379

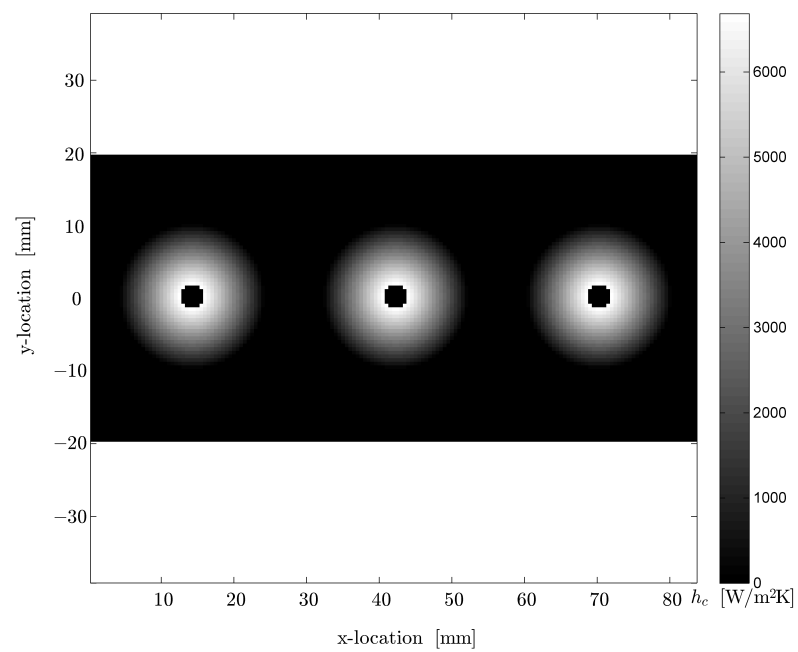


Figure C.7: Resulting thermal contact conductance across the interface, used in the numerical simulation for three bolts.

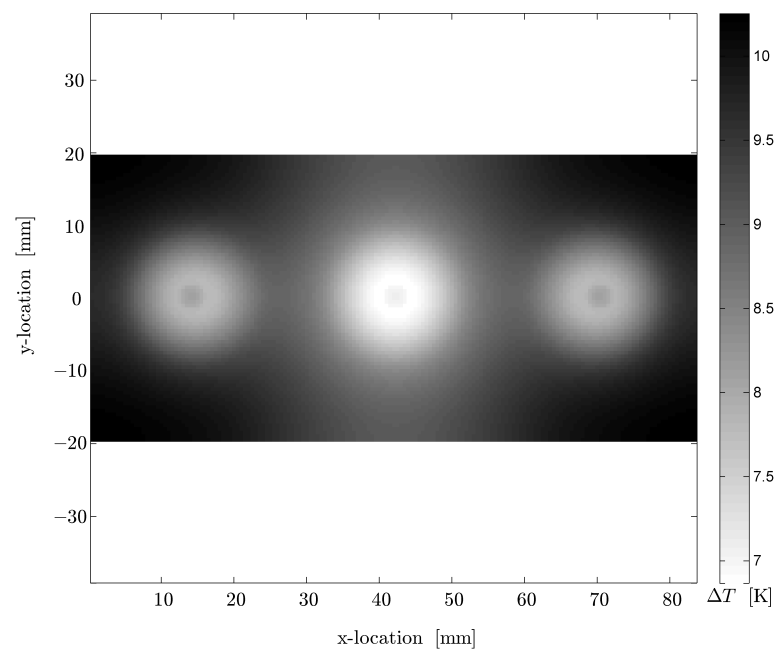


Figure C.8: Resulting interface temperature drop from numerical simulations using the thermal contact conductance distribution presented in Figure C.7.

APPENDIX D

Microhardness Measurements

This chapter presents the results from the performed microhardness measurements, described in Section XX. Figure D.1 shows resulting Vickers hardness for four different applied loads; 0.05, 0.1, 0.2 and 0.5 kg. For this interval of applied loads, the Vickers hardness was found to decrease with increasing load, which was in accordance with previously conducted tests [21]. As can be seen, the Vickers hardness converges to a constant value of approximately 1.7 GPa, which corresponds to the surface macrohardness.

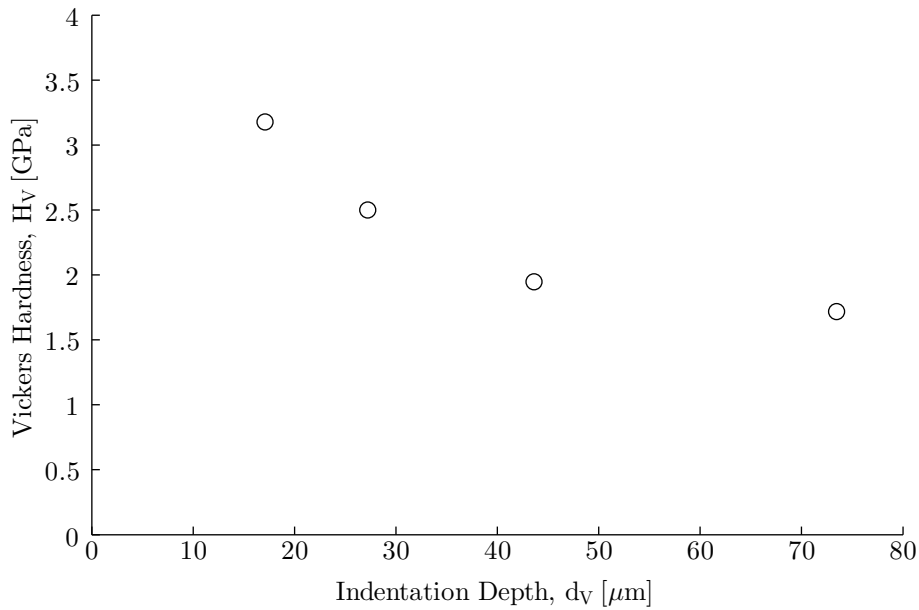


Figure D.1: Measured Vickers hardness and indentations diagonal for loads of 0.05, 0.1, 0.2 and 0.5 kg. The Vickers hardness is decreasing with increasing load.

The three first measurement points in Figure D.1 were considered to belong to the microhardness region, where the Vickers hardness is a non-constant function of indentation depth. The fourth measurement point was considered to belong to the macrohardness

region. Figure D.2 shows the measured values together with least squares curve given by equation 2.33, with $c_1 = 14.0$ GPa and $c_2 = -0.52$. Equation 2.31 for the relative contact pressure can now be written as

$$\frac{P}{H_c} = \left[\frac{P}{22.7 \cdot 10^9 (\sigma_s / \sigma_0 m)^{-0.52}} \right]^{1.039} \quad (\text{D.1})$$

where $\sigma_0 = 1 \mu\text{m}$. Equation D.1 was used for all plastic models for thermal contact conductance described in Section 2.3.3.

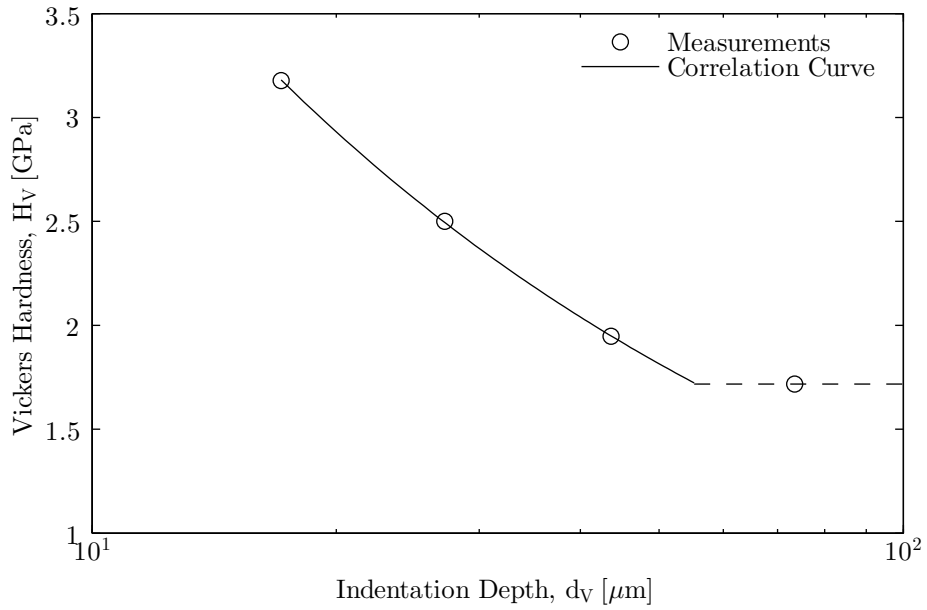


Figure D.2: Microhardness correlation curve based on measured values of Vickers hardness. The solid and dashed lines cover the microhardness and macrohardness region, respectively.

APPENDIX E

Roughness Measurements

The resulting values of arithmetic average of absolute values of surface roughness, R_a , RMS surface roughness, σ and absolute surface slope, m , are given in Table E.1 for all tested surfaces. The relationship between σ and R_a assuming Gaussian distribution of surface asperities (Section 2.3.1), $\sigma \approx 1.25R_a$, holds well for the results in Table E.1.

Table E.1: Measured surface roughness parameters R_a and σ together with absolute surface slope m for all interface surfaces of the bolted joint and cylinder joint experiment.

Configuration	R_a [μm]	σ [μm]	m
No.1, top	0.35	0.44	0.049
No.1, bottom	0.36	0.45	0.043
No.2, top	0.54	0.68	0.038
No.2, bottom	0.72	0.88	0.032
No.3, top	0.24	0.31	0.027
No.3, bottom	0.32	0.41	0.033
No.4, top	0.69	1.08	0.65
No.4, bottom	0.38	0.59	0.25
Cyl., top	0.31	0.39	0.16
Cyl., bottom	0.39	0.51	0.16

APPENDIX F

Model Parameters

Listed below in Table F.1 are the values of the model parameters used when calculating estimations of thermal contact conductance in Section 4.3.

Table F.1: Values of model parameters

Parameter	Value	Unit
E	200	[GPa]
E'	221.3	[GPa]
ν	0.31	[-]
k	90.9	[W/mK]
R_a	0.35	[μm]
m_s	0.23	[-]
σ_s	0.64	[μm]
FD	10	[μm]
δ_0	0.95	[μm]
r	0.005	[m]
α	13.4	[$\mu\text{m}/\text{mK}$]
$T_{m,1}$	283.4	[K]
$T_{m,2}$	286.9	[K]
$T_{m,3}$	294.5	[K]
$T_{m,4}$	302.1	[K]
$T_{m,5}$	300.8	[K]